D2.4 Validation of early design tools for agri-PV systems

Symbiosyst

Horizon Europe EU project
Grant Agreement No. 101096352



Funded by the European Union

Funded by the European Union. Views and opinions expressed are however those of the author(s) only and do not necessarily reflect those of the European Union or CINEA. Neither the European Union nor the granting authority can be held responsible for them. As of 11th of November 2026 this report has been submitted to the EC but its content has not been approved yet

Document control sheet

Project	**SYMBIOSYST – Create a Symbiosis where PV and agriculture can have a mutually beneficial relationship**

Topic identifier	HORIZON-CL5-2022-D3-01-06
Grant Agreement N°	101096352
Coordinator	ACCADEMIA EUROPEA DI BOLZANO (EURAC)
Duration	01/01/2023 – 31/12/2026
Work package N°	WP2
Work package title	Robust and replicable design of novel and sustainable agri-PV solutions
Work package leader	LUCISUN
Task n°	2.4
Task leader	EURAC
Document title	Validation of early design tools for agri-PV systems
Lead Beneficiary	EURAC
Dissemination level	PUBLIC
Authors	Giovanni Borz, Jonathan Leloux
Contributors	
Reviewer(s)	Jodie Isa
Issue date	11/11/2026

History of versions

Version	Date	Author - Beneficiary	Comments
V1.0	11/11/2026	Giovanni Borz, Jonathan Leloux, Jodie Isa	Final version

Acknowledgements

The work described in this publication has received funding from the European Union Horizon Europe research and innovation programme under grant agreement Nº 101096352.

Disclaimer

This work may rely on data from sources external to the members of the SYMBIOSYST project Consortium. Members of the Consortium do not accept liability for loss or damage suffered by any third party as a result of errors or inaccuracies in such data. The information in this document is provided “as is” and no guarantee or warranty is given that the information is fit for any particular purpose. The user thereof uses the information at its sole risk, and no member of the SYMBIOSYST Consortium shall be liable for any use that may be made of the information.

Table of contents

Document control sheet 2

Acknowledgements 3

Disclaimer 3

Table of contents 4

List of Figures 6

List of tables 7

Acronyms and Abbreviations 8

Executive Summary 10

Introduction 11

DualHarvest (Agri-PV Early Design Tool) 11

Description of the Tool *11*
How the *DualHarvest* model works 11

Validation *14*
Methodology 14
Results 19
Discussion 21

LUSIM: 3D irradiance simulation on simplified customizable Agri-PV system 21

Introduction *21*

Methodology *23*
Baseline and fixed parameters 23
Configurable interface and model catalogue 25
Scene generation and coupled parameter changes 26
PV modules and surface properties 27
Surface sampling and spatial averaging 28
Mesh complexity and PV sampling 29
Spatial means and comparison indicators 30
Configuration matrix 30
Representative days and monthly profiles 31
Recorded computation time 32

Results *33*
Annual irradiation 33
B01 — Baseline light distribution 34
B02 — Backtracking and the annual radiation balance 35
Backtracking on winter and summer days 36

Backtracking during transition seasons 37
Monthly average daily profiles 38
B03 — Tracker pitch and land-use implications 39
B04 — Tracker height and vertical separation 40
B05 — Crop size and daily light distribution 40
B06 and B08 — Bifacial rear resource and ground albedo 42
B07 and B09 — Crop geometry and tracker rotation range 44
B09 — Maximum tracker rotation 46
B07-b — Module selection with Crop Model 1 46
Seasonal and daily module response 47
B13 — Crop count and rear irradiation 48
Seasonal and daily crop-count response 50
B10–B12 — Complexity and computation time 51
Application runtime and hardware 53

Discussion *54*
Implications for early design 54
Use of irradiance outputs in crop models 54
Limitations 55

Aerial Agri-Topography: UAV-derived site models for Agri-PV early design **55**

Introduction *55*

Methodology *56*

Results *56*

Discussion *58*

Conclusions **59**

References **60**

List of Figures

Figure 1. Complete model of an Agri-PV included in the Context (Large View).....13
Figure 2: Positioning of the front- and rear-facing pyranometers on the tracker structure at the Bolzano demonstrator. 17
Figure 3: Comparison between measured and simulated irradiance values on the front and rear sides of the photovoltaic modules for the test day on 23 May 2026.....19
Figure 4: Comparison between measured and simulated irradiance values on the front and rear sides of the photovoltaic modules for the test day on 11 June 2026. 20
Figure 5: Comparison between measured and simulated irradiance values on the front and rear sides of the photovoltaic modules for the test day on 04 July 2026.....20
Figure 6: Generic configurable agrivoltaic scene. Illustration of the simplified array and crop objects. 23
Figure 7: Configurable inputs in LUSIM. The panel shows the B01 settings, including Type 2 modules, Crop Model 2, 5 m pitch and 4.7 m tracker height.....25
Figure 8: OBJ import menu in the internal LUSIM interface. This menu provides context for the model catalogue and is not available in the configurable early-design interface.....25
Figure 9: Simplified crop geometries. Left: the branched geometry shown for Model 2. Right: the tapered geometry shown for Model 1. The object meshes determine receiving surfaces and self-obstruction.....28
Figure 10: PV mesh complexity. Supplied illustration of low, medium and high PV triangulation. The assessed low and high settings use nominal vertex spacings of 1 m and 0.25 m. The medium setting is shown for context and is not part of the reported comparison.....29
Figure 11: Baseline monthly radiation components. Each panel uses its own vertical scale. Values are monthly mean daily irradiation. 34
Figure 12: Monthly backtracking comparison. B02 relative to B01. Upper panels show mean daily irradiation; lower panels show monthly percentage changes. 35
Figure 13: January backtracking examples. Upper row: clear-sky day 21 January. Lower row: overcast day 4 January. 36
Figure 14: June backtracking examples. Upper row: clear-sky day 23 June. Lower row: overcast day 16 June. 36
Figure 15: March backtracking examples. Upper row: clear-sky day 31 March. Lower row: overcast day 4 March. 37
Figure 16: October backtracking examples. Upper row: clear-sky day 20 October. Lower row: overcast day 15 October.....37
Figure 17: Mean January and June daily profiles. All days in each month are included. Hour 12 denotes the highest-elevation sample of each day.....38
Figure 18: Pitch comparison with backtracking. B03 pitches of 6, 9 and 12 m.....39
Figure 19: Tracker-height comparison. B04 heights of 4.1, 4.25 and 5.25 m, with backtracking enabled and 36 crop instances. 40
Figure 20: Crop-height comparison. B05 heights of 2, 3 and 4 m. Uniform scaling changes the whole crop geometry.....41
Figure 21: Geometry responses on June example days. Upper row: clear-sky day 23 June. Lower row: overcast day 16 June.....42
Figure 22: Type 1 module scene. Mono144 modules above Crop Model 2. The screenshot illustrates the configuration; its colours have no supplied quantitative legend.....43

Figure 23: Seasonal and daily albedo response. Left: monthly mean daily rear irradiation. Right: percentage changes on the selected clear-sky day and overcast day days. 44
Figure 24: Crop Model 1 geometry. The wider crop crown changes the receiving surface and obstruction around the modules. 45
Figure 25: Monthly crop-model and rotation comparisons. B07 and B09 compared with B01. 45
Figure 26: B07-b scene with Mono144 modules. Three modules and two crop objects per table. The image has no timestamp or quantitative colour legend. 47
Figure 27: Monthly module-selection response. B07-b versus B07, with Crop Model 1 and two crops per table. 47
Figure 28: Module response on June example days. Upper row: clear-sky day 23 June. Lower row: overcast day 16 June. 48
Figure 29: Three-crop configuration. B13 scene showing the denser planting arrangement. The image is labelled 21 June at 13:16 local time. 49
Figure 30: Monthly crop-count response. B13 versus B07-b, with Mono144 and Crop Model 1. 50
Figure 31: Crop-count response on June example days. Upper row: clear-sky day 23 June. Lower row: overcast day 16 June. 50
Figure 32: Monthly complexity comparison. B01 high/high compared with B10 low/high, B11 high/low and B12 low/low. 51
Figure 33: Recorded runtime for complexity settings. Each value is a single-run observation on the reference computer. 51
Figure 34: Topographic map of the Bolzano demonstrator with apple tree positions and contour lines [17]. 57
Figure 35: 3D model of the Bolzano demonstrator showing PV modules and tree structures [17]. 58

List of tables

Table 1. Example of the output for the Electrical Production Simulation 14
Table 2: Example of Optical Parameters of a material 15
Table 3: Baseline Configuration 24
Table 4: Relationship between scene inputs and generated geometry 26
Table 5: Built-in PV module properties 27
Table 6: Simulation cases and comparison references 31
Table 7: Days selected for detailed comparison 31
Table 8: Annual irradiation in kWh/m²/year 34
Table 9: Monthly backtracking changes relative to B01 38
Table 10: Albedo effect on annual rear irradiation 43
Table 11: B07 and B07-b module comparison 46
Table 12: Annual effect of increasing crop count 49
Table 13: Complexity response relative to B01 51
Table 14: Computer used for the simulations 53
Table 15: Recorded application runtime 53
Table 16: Topographic survey specification and Bolzano campaign settings 56

Acronyms and Abbreviations

3D	Three-dimensional
Agri-PV / agri-PV	Agrivoltaics / agri-photovoltaics
AGL	Above ground level
BNI	Beam Normal Irradiance
BRDF	Bidirectional Reflectance Distribution Function
BTDF	Bidirectional Transmittance Distribution Function
CAPEX	Capital Expenditure
CINEA	European Climate, Infrastructure and Environment Executive Agency
CSV	Comma-Separated Values
D6.2	Deliverable 6.2
DEM	Digital Elevation Model
DHI	Diffuse Horizontal Irradiance
DLI	Daily Light Integral
DNI	Direct Normal Irradiance
DSM / DTM	Digital surface model / Digital terrain model
EC	European Commission
EIA	Environmental Impact Assessment
EPW	EnergyPlus Weather file
EU	European Union
GA	Grant Agreement
GCP	Ground control point
GNSS	Global navigation satellite system
GPU	Graphics Processing Unit
GCR	Ground coverage ratio
GSD	Ground sampling distance
Kd	Diffuse reflectance coefficient
Kp	Effective number of surface passes
Ks	Specular reflectance coefficient
Kt	Total transmittance
kV	Kilovolt
LCOE	Levelized Cost of Energy
LED	Light-Emitting Diode
LiDAR	Light Detection and Ranging
MASE	Ministry of the Environment and Energy Security
MTL	Material Template Library / material file
MW	Megawatt
NOCT	Nominal Operating Cell Temperature
nRMSE	Normalized Root Mean Square Error
Ns	Shininess coefficient
OBJ / .obj	Wavefront OBJ file
OPEX	Operating Expenditure

PAR	Photosynthetically Active Radiation
PPFD	Photosynthetic Photon Flux Density
PR	Performance Ratio
PV	Photovoltaic
PVGIS	Photovoltaic Geographical Information System
RTK / NRTK	Real-time kinematic / Network real-time kinematic
RMSE	Root mean square error
SANDIA	Sandia National Laboratories
TIN	Triangulated irregular network
TMY	Typical Meteorological Year
UAV	Unmanned aerial vehicle
USCS	Unified Soil Classification System
VPD	Vapour Pressure Deficit
WACC	Weighted Average Cost of Capital
WEA	Weather file format for Radiance workflow
WP6	Work Package 6
$W \cdot m^{-2}$	Watts per square metre
$\mu mol \cdot m^{-2} \cdot s^{-1}$	Micromoles per square metre per second
$mol \cdot m^{-2} \cdot d^{-1}$	Moles per square metre per day
°C	Degree Celsius
m / m^2	Metre / square metre
h	Hour

Executive Summary

This deliverable presents the simplified agrivoltaics modelling approach developed in SYMBIOSYST to support early-stage stakeholder understanding of agri-PV design options. The deliverable documents three complementary components: the EURAC early-design tool (*DualHarvest*), which supports rapid screening of agri-PV configurations, and the public LUSIM demo provided by LUCISUN, which enables more detailed visualisation and analysis of irradiance distribution in selected open-field and greenhouse scenarios and the UAV-based topographic and 3D site-modelling workflow developed by ABOVE, which supports the characterisation and digital representation of agri-PV sites.

Introduction

This deliverable presents the validation study of the two early-design tools developed within the SYMBIOSYST project, DualHarvest and LUSIM. The document first provides a general description of both tools, outlining their main functionalities, the required input data, and the outputs generated.

Subsequently, the methodologies adopted for the validation of the models are presented. This section describes the validation approach, the methodological choices made during the process, and the experimental datasets used to assess the performance of each tool. Particular attention is given to the selection and processing of the experimental data and to their use as reference data for model validation.

Finally, the deliverable provides an assessment of the accuracy and reliability of the simulation results by comparing the model predictions with the corresponding experimental measurements. This analysis aims to evaluate the extent to which the tools are able to reproduce the observed conditions and to identify potential discrepancies between simulated and measured data. The results will also be critically discussed to identify the main limitations of the models, including potential sources of uncertainty and aspects that may affect their applicability under different operating and environmental conditions. This discussion will provide a basis for understanding the current capabilities of the tools and identifying potential areas for future improvement.

DualHarvest (Agri-PV Early Design Tool)

Description of the Tool

The tool developed by Eurac is designed to provide an initial assessment of the potential electricity yield and the amount of light reaching the various parts of the plant, the ground and the photovoltaic modules. As this tool is specifically designed for users with no prior experience of 3D modelling or light simulation, it is designed to be user-friendly. The target user is primarily a farm owner or an agronomist. This is because, when speaking with these professionals, we realised that in the early stage of designing an Agri-PV system, the two main questions asked upfront are: the potential for electricity generation, and, most important, the amount of light reaching the plants and the soil near the plants (the latter to assess soil evapotranspiration).

How the *DualHarvest* model works

To achieve the intended simulation results, the model carries out the following main steps:

User Inputs

1. The user is first asked to provide some parameters to build the 3D model of the Agri-PV system. The parameters are:

a. The shape of the plant's foliage, to be chosen among 4 options:
    i. Hexagonal pyramid
    ii. Hexagonal prism
    iii. Hexagonal bipyramid
    iv. Inverted hexagonal pyramid
b. Total height of the plant and height of the trunk.
c. Canopy width of the plants.
d. Distance between two rows of plants.
e. Distance between two plants in the same row.
f. The height of the vertical posts of a single tracker and the length of the horizontal beam of a tracker.
g. The thickness of the vertical and horizontal posts of the tracker structure.
h. Number of vertical posts per tracker.
i. Number of rows of plants between each tracker.
j. Height of the anti-hail net
k. Geolocation of the Agri-PV plant and direction of the Trackers respect to North.

The optical characteristics of the plants and photovoltaic modules models – such as the transparency percentage of the modules and the canopy, or the colour of the canopy or ground – can also be adjusted quite easily by editing a text file. In any case, the tool provides default values so that even a non-expert user can still run a simulation.

2. Module specifications:
    a. Efficiency
    b. Width
    c. Length
    d. Thickness
    e. Bifaciality factor
    f. Transparency
    g. Temperature coefficient (default value if not entered by the user)

3. Input of weather data from a file (EPW format)

4. The user decides on the parameters of the simulation.
    These parameters are:
    a. Timestep
    b. Start and end date and time of the simulation
5. Optional inputs:
    a. Context OBJ file
    b. CAPEX and OPEX values
    c. Lifetime of the plant
    d. WACC (Weighted Average Cost of Capital)

These inputs are defined as optional because the code can run even without these values being provided by the user. Specifically, the simulation can be run even without context files, in which

case only the geographical location is taken into account, rather than the shading caused by the topographical profile of the area surrounding the Agri-PV plant. As regards CAPEX, OPEX and lifetime values, the code uses default values generated by the Symbiosyst project, which are therefore close to realistic figures.

Tool Workflow

The workflow of the tool begins with the generation of a parametric 3D model of the Agri-PV system, including photovoltaic trackers, PV modules, crop geometries, and the surrounding environment. The geographical context,in OBJ format, is imported from external sources such as Digital Elevation Models (DEMs), LiDAR datasets, photogrammetric reconstructions, or online mapping services, allowing the simulation to account for terrain-induced shading and horizon obstruction effects (Figure 1).

Based on the geometry generated, dedicated meshes are automatically created for PV modules, ground surfaces, and crop canopies. These meshes serve as measurement surfaces for the irradiance simulations and are generated according to user-defined spatial resolutions. Material properties are assigned through a unified material library and automatically translated into Radiance-compatible definitions to ensure consistent optical behaviour during ray-tracing calculations.

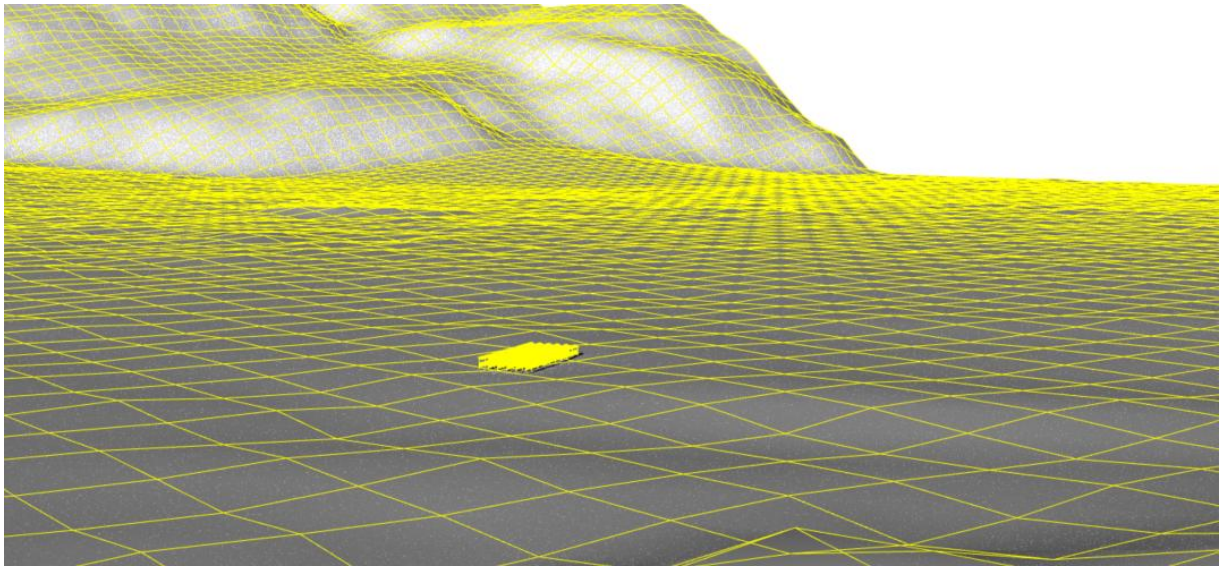


Figure 1. Complete model of an Agri-PV included in the Context (Large View)

Meteorological conditions are represented through dynamic sky generation. For each simulation timestep, weather data from EPW files are processed to create physically consistent Radiance sky models based on the corresponding solar position and atmospheric conditions.

The irradiance simulation is performed using Radiance and can operate in two different modes. In standard operation, tracker positions follow the conventional sun-tracking strategy. Alternatively, an optimization mode allows tracker movements to be adjusted in order to satisfy crop-specific irradiation requirements while minimizing deviations from the reference solar-tracking configuration and preserving photovoltaic energy production.

Simulation outputs are subsequently used to estimate the electrical energy generated by the Agri-PV system. Energy production is calculated through simplified bifacial photovoltaic models, with the option to include temperature corrections based on the Nominal Operating Cell Temperature (NOCT) methodology. For annual simulations, the workflow additionally computes the Levelized Cost of Energy (LCOE), providing a preliminary economic assessment of the proposed configuration.

The final outputs are provided in tabular formats, such as Excel spreadsheets, reporting irradiance levels, tracker positions, electrical energy production, and economic indicators. This approach ensures rapid interpretation of results and facilitates their integration into subsequent design, analysis, and decision-making processes (Table 1).

datetime	angle_deg	angle_str	module_top_\	module_bottom_'	plant_upper_east_V	plant_upper_west_	plant_lower_e	plant_lower_v	ground_far_r	ground_mid_	ground_near_	ground_left_f	ground_lef	ground_lef	ground_rig	ground_rig	ground_rig	electrical_production_kWh
01.06.24 05:00	2	-2deg	0.029842834	2.39E-05	0.000133333	6.67E-05	0.000133333	6.67E-05	0.0294	0.0294	0.0294	0.0295	0.0295	0.0294	0.0293	0.0293	0.0294	0.00031
01.06.24 05:30	6	-6deg	74.6822874	17.0497833	215.7838667	95.40326667	0.260966667	0.03243333	61.1489	33.3191	61.1489	61.1139	61.1303	61.1466	61.1839	5.5079	61.1512	0.90221
01.06.24 06:00	12	-12deg	130.2839042	18.72235116	0.017233333	0.038366667	0.0173	0.03836667	7.4335	7.4335	108.7879	7.3865	7.4085	108.7848	7.4805	7.4585	108.791	1.49297
01.06.24 06:30	16	-16deg	230.7209088	0.605329916	276.9854667	0.5981	0.019166667	0.59823333	202.51745	104.4916	202.51745	202.4757	6.4435	202.5147	202.5592	202.5397	202.5202	2.40487
01.06.24 07:00	22	-22deg	278.0896546	2.890547344	268.0288333	2.3559	0.041033333	2.35583333	258.76705	258.767	258.76705	258.7513	258.7586	258.766	258.7828	258.7754	258.7681	2.91447
01.06.24 07:30	28	-28deg	365.1456012	8.526003805	0.074566667	0.185833333	0.074666667	0.1858	374.0657	187.71615	1.3665	374.0688	1.3682	1.3667	374.0626	374.0641	1.3663	3.86159
01.06.24 08:00	34	-34deg	379.5896283	15.32187378	0.046133333	0.030133333	0.0462	0.03016667	440.2501	440.2501	1.8356	440.254	440.2522	1.8359	440.2462	440.248	1.8353	4.06177
01.06.24 08:30	38	-38deg	405.1731998	24.07329747	0.050233333	0.0869	0.050333333	0.08696667	530.6838	267.1785	3.67325	530.7075	530.6964	3.6748	530.6601	3.6606	3.6717	4.39222
01.06.24 09:00	44	-44deg	380.7285853	36.04361876	0.066533333	0.086566667	0.0666	0.08666667	587.5148	294.676	1.8372	587.524	587.5197	1.8378	587.5056	1.8323	1.8366	4.2258
01.06.24 09:30	50	-50deg	355.2447702	50.50951585	0.1346	0.146733333	0.1346	0.14686667	673.13645	673.1364	1.4371	673.1415	673.1391	1.4374	673.1314	673.1337	1.4368	4.06691
01.06.24 10:00	50	-50deg	359.1199067	55.4232829	0.401166667	0.1284	0.401	0.12853333	722.70305	363.6632	363.6632	722.7325	722.7187	722.7049	722.6736	4.6077	4.6215	4.14331
01.06.24 10:30	50	-50deg	379.8152448	62.08933166	0.366433333	165.0489667	0.3664	0.1816	798.33475	402.56335	402.56335	798.376	798.3568	798.3375	798.2935	6.7699	6.7892	4.40758
01.06.24 11:00	50	-50deg	382.5232554	64.97463357	0.421966667	175.7884	0.4218	0.1553	826.87065	416.54535	416.54535	826.9117	826.8925	826.8733	826.8296	6.1982	6.2174	4.45695
01.06.24 11:30	50	-50deg	359.6396142	62.4387641	0.213133333	170.9911333	0.2132	0.20026667	791.0956	398.3975	791.0956	791.1286	791.1132	791.0977	791.0626	5.6818	791.0935	4.20024
01.06.24 12:00	44	-44deg	433.8170623	53.81849767	0.2572	173.5784333	0.257166667	0.1436	798.15245	401.88045	798.1525	798.1892	798.1721	798.1549	798.1157	5.5888	798.1501	4.90868
01.06.24 12:30	22	-22deg	652.2905285	7.214618184	91.58736667	329.4394333	0.302166667	0.17323333	788.68005	397.24925	788.68005	788.7189	788.7007	788.6826	788.6412	5.7978	788.6775	6.83941
01.06.24 13:00	-12	-12deg	713.9048118	80.3618861	155.3336333	347.1320667	0.4225	0.28236667	774.856	390.08645	774.85605	774.8859	774.8719	774.858	774.8261	5.301	774.8541	8.01764
01.06.24 13:30	-30	-30deg	579.2354123	21.489514	187.8469	425.6794667	0.4596	0.16773333	774.44735	390.4494	390.44945	774.486	774.4679	774.4499	774.4087	6.4309	6.449	6.18418
01.06.24 14:00	-38	-38deg	489.5605898	36.1023192	219.3149	396.3186	4.330066667	0.27043333	739.49825	372.39105	372.39105	739.5317	739.5161	739.5005	739.4648	5.266	5.2816	5.35852
01.06.24 14:30	-40	-40deg	442.8690222	35.11295969	0.2213	356.0314667	0.2212	0.12743333	671.67255	671.6725	2.28405	671.6857	671.6795	2.2849	671.6594	671.6655	2.2832	4.86548
01.06.24 15:00	-40	-40deg	428.5578914	30.92899216	0.104066667	110.9079	0.1041	0.10636667	621.00015	621.00015	311.26875	621.0042	621.0023	621.0004	620.9961	620.998	1.5371	4.68586
01.06.24 15:30	-38	-38deg	404.0571615	22.77590671	0.075433333	0.072733333	0.0755	0.0728	537.92855	270.69915	3.46975	537.9507	537.9404	3.4712	537.9064	3.4579	3.4683	4.37108
01.06.24 16:00	-36	-36deg	393.2980111	16.88328326	0.045133333	0.055633333	0.045133333	0.0557	476.1161	476.1161	2.2508	476.1283	476.1226	2.2516	476.1039	476.1096	2.25	4.21586

Table 1. Example of the output for the Electrical Production Simulation

Validation

Methodology

3D Model

The most critical component of the modelling framework is the irradiance simulation part, which is responsible for calculating the spatial distribution of solar irradiance on the different surfaces represented within the three-dimensional model. As the accuracy of this component directly affects all subsequent analyses, including crop light availability and PV energy yield assessments, a dedicated validation activity was undertaken.

To perform this validation, at first a detailed digital replica of the Bolzano agrivoltaic demonstrator was developed. The model was reconstructed with a level of detail sufficient to accurately represent the main elements influencing solar radiation interception and shading patterns. In particular, the following components were included:

- Vertical support poles;
- Horizontal rotating beam
- PV modules and mounting structures;
- Ground surface;
- Tree rows and canopy geometry.
- Surrounding mountain profiles, represented to account for horizon obstruction effects

The resulting digital model was used as the basis for the irradiance simulations and served as the reference geometry for the comparison between simulated and measured irradiance data. By recreating the physical characteristics of the demonstrator as accurately as possible, the validation focused specifically on evaluating the capability of the modelling framework to reproduce the actual irradiance conditions observed in the field.

Optical Properties

Optical properties were assigned to each component of the digital scene, including the ground surface, vegetation canopy, PV modules, and structural elements. These properties were derived from a combination of values reported in the scientific literature and site-specific data obtained through drone-based surveys. The latter provided detailed information on the characteristics of the demonstrator, supporting a more realistic parameterisation of the model and enhancing the accuracy of the simulated irradiance distribution.

To ensure a realistic representation of radiative interactions within the simulated environment, optical properties were assigned to all materials composing the three-dimensional scene. These properties describe how each surface interacts with incident solar radiation through reflection, transmission, and absorption processes, and are essential for accurately reproducing irradiance conditions within the agrivoltaic system.

The modelling framework requires material properties to be defined through a Wavefront Material Library (.mtl) file associated with the three-dimensional geometry. Each object contained in the scene is linked to a specific material definition, allowing different optical behaviours to be assigned to vegetation, ground surfaces, structural elements, and photovoltaic modules.

The optical parameters were derived from a combination of literature values and site-specific information obtained through UAV-based surveys of the demonstrator. This approach allows the radiative properties of the simulated scene to closely match the actual characteristics of the installation.

An example of a material definition is reported in Table 2:

Parameter	Value
Material name	Example tree_leaves
Kd	(0.090, 0.200, 0.080)
Kt	(0.130, 0.130, 0.130)
Kp	2
Ks	(0.030, 0.050, 0.030)
Ns	80
d	1.000
Ni	1.000

Table 2: Example of Optical Parameters of a material

where:

- **newmtl**: defines the name of the material;
- **Ka** (*ambient reflectance*): describes the material response to ambient illumination;
- **Kd** (*diffuse reflectance*): defines the fraction of incident light diffusely reflected by the surface. The three values correspond to the red, green, and blue spectral channels;
- **Ks** (*specular reflectance*): represents the specular or mirror-like component of reflected light;
- **Ns** (*shininess exponent*): controls the concentration of specular reflections. Higher values correspond to smoother and more reflective surfaces;
- **d** (*opacity*): defines the transparency of the material, with values ranging from 0 (fully transparent) to 1 (fully opaque);
- **Ni** refraction index

For vegetation elements, the diffuse reflectance values were selected to reproduce the optical response of the tree canopy observed at the demonstrator site. Similarly, dedicated material definitions were assigned to photovoltaic modules, support structures, and ground surfaces based on their respective optical characteristics. Through this material-based parameterisation, the model is able to reproduce the main radiative processes occurring within the agrivoltaic system and provide a reliable basis for irradiance simulations.

To validate the model, irradiance was calculated at the same locations where pyranometers were installed in the pilot system. In particular, the analysis considered the two pyranometers mounted on the rotating beam of the tracker structure and mechanically coupled to the rotation of the PV modules. This configuration ensures that the sensors continuously follow the orientation of the modules during tracker operation.

The two sensors were installed on opposite sides of the rotating beam: one pyranometer was mounted on the upper side of the structure, measuring the incident irradiance on the front-facing surface, while the second pyranometer was mounted on the lower side, measuring the irradiance reaching the rear-facing surface. This setup enables the simultaneous assessment of irradiance conditions on both sides of the agrivoltaic structure and provides a valuable dataset for validating the capability of the model to reproduce the dynamic shading and reflection effects associated with tracker movement (Figure 2).

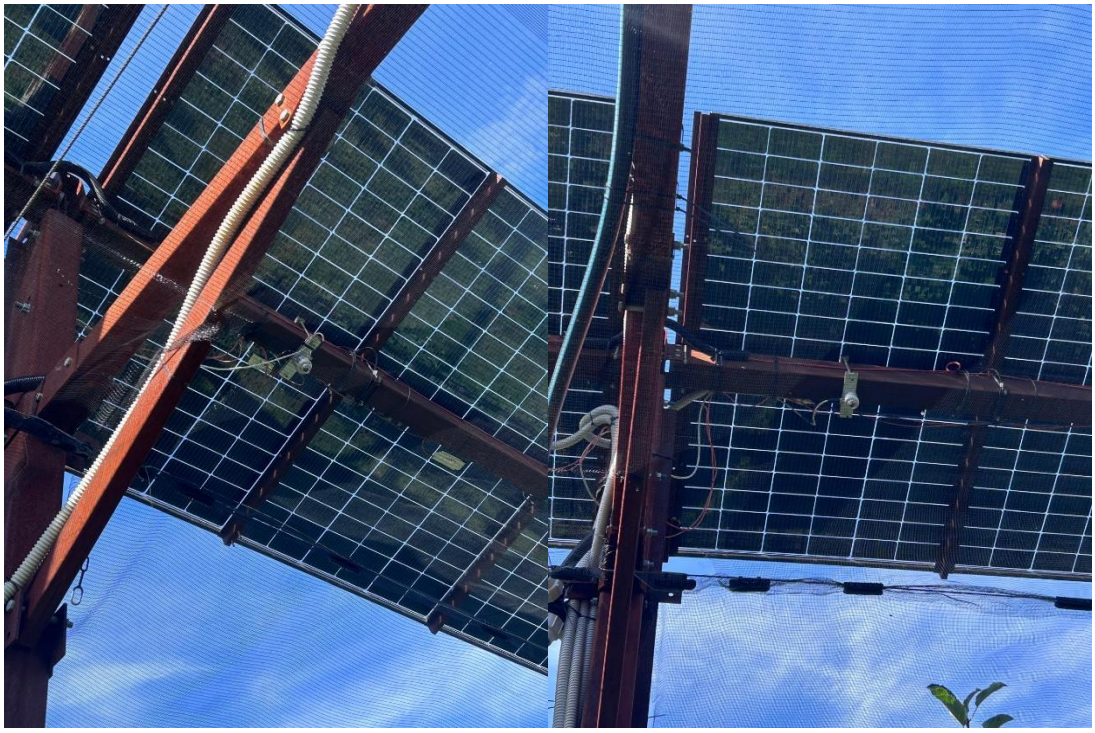


Figure 2: Positioning of the front- and rear-facing pyranometers on the tracker structure at the Bolzano demonstrator.

Within the digital model, virtual sensor points were positioned at locations corresponding to the physical pyranometer installations. Simulated irradiance values were then extracted for these positions and compared with the measured data over the selected validation period. This approach allowed the accuracy of the irradiance simulation engine to be quantitatively evaluated under real operating conditions.

Validation Period

To assess the performance of the irradiance modelling framework, the validation was performed using data from three representative clear-sky days selected during the growing season, specifically in May, June, and July. These months correspond to a critical period for crop development, when the canopy reaches its maximum extent and solar radiation availability becomes a key factor influencing plant growth and productivity.

The validation focused exclusively on clear-sky conditions to minimize uncertainties associated with the meteorological input data and to ensure a reliable comparison between measured and simulated irradiance values. The irradiance simulations were driven by weather data acquired from a meteorological station located approximately 10 km from the Bolzano agrivoltaic demonstrator. While such a distance is generally acceptable under stable atmospheric conditions, local cloud formation and spatial variability in irradiance can introduce discrepancies between the conditions recorded at the weather station and those experienced at the demonstrator site, particularly in mountainous environments such as South Tyrol.

The selection of clear-sky days reduces these atmospheric uncertainties and allows the validation to focus on the core components of the modelling framework, including the geometric representation of the agrivoltaic system, solar position calculations, tracker operation, shading patterns, and radiation interactions with the crop canopy.

The chosen period is particularly relevant for agrivoltaic applications because the fully developed canopy represents the most challenging condition for light distribution within the system. During late spring and summer, increased foliage density enhances light interception by the crop and modifies the spatial distribution of irradiance below the photovoltaic structures. Consequently, this period provides the most stringent test of the model's ability to reproduce irradiance dynamics both above and within the plant canopy, where accurate light characterization is essential for assessing potential impacts on crop performance.

By concentrating the validation on representative clear-sky days during the peak growing season, the analysis provides a robust assessment of the model's capability to reproduce irradiance conditions under the most agronomically relevant and structurally complex operating scenarios of the agrivoltaic system. Finally, the dataset acquired from the demonstrator sector featuring multi-axis trees and PV modules with standard transparency was selected for the validation of the developed model.

The three representative days were selected for the validation:

- **4 July 2026**: summer clear-sky day;
- **11 June 2026**: early summer clear-sky day;
- **23 May 2026**: spring clear-sky day.

Simulations

For each of the selected validation days, irradiance simulations were performed using a temporal resolution of 30 minutes. The resulting irradiance values at the virtual sensor locations were then compared with the measurements recorded by the corresponding pyranometers installed at the pilot site. This comparison enabled the evaluation of the model accuracy under different seasonal and atmospheric conditions, ranging from direct-radiation-dominated clear-sky days to diffuse-radiation.

Particular attention was devoted to assessing the limitations associated with the simplified representation of vegetation adopted within the modelling framework. While simplified canopy models significantly reduce computational effort and facilitate the generation of digital scenes, they may not fully capture the complexity of real tree architectures, including the heterogeneous distribution of foliage, gaps within the canopy, and variations in optical properties. The validation exercise therefore aimed not only to quantify the agreement between simulated and measured irradiance values but also to identify the extent to which such simplifications affect the accuracy of irradiance predictions. The results provide valuable insights into the applicability of the proposed modelling approach and highlight potential areas for future refinement of vegetation representation within agrivoltaic simulations.

Results

To evaluate the accuracy of the developed irradiance modelling workflow, the simulation results were compared against measurements collected at the demonstrator site during three representative clear-sky days. The validation focused on the irradiance incident on both the front and rear sides of the photovoltaic modules, allowing the assessment of the model's capability to reproduce the temporal evolution of the solar resource under real operating conditions.

For each validation day, simulated and measured irradiance values were compared on a timestep-by-timestep basis throughout the entire daylight period. The analysis considered both the irradiance received by the upper surface of the PV modules and the irradiance received by the lower surface, which is particularly relevant for bifacial photovoltaic systems where rear-side irradiance contributes to the overall energy yield.

Figure 3- Figure 5 present the comparison between measured and simulated irradiance values for the three analysed days. In each figure, the temporal profiles obtained from the simulation are plotted together with the corresponding measurements, enabling a direct evaluation of the model performance across different solar positions and irradiation levels.

Overall, the comparison provides a quantitative assessment of the model's ability to reproduce the irradiance conditions experienced by the photovoltaic modules and to accurately represent both front-side and rear-side radiation components.



Figure 3: Comparison between measured and simulated irradiance values on the front and rear sides of the photovoltaic modules for the test day on 23 May 2026.

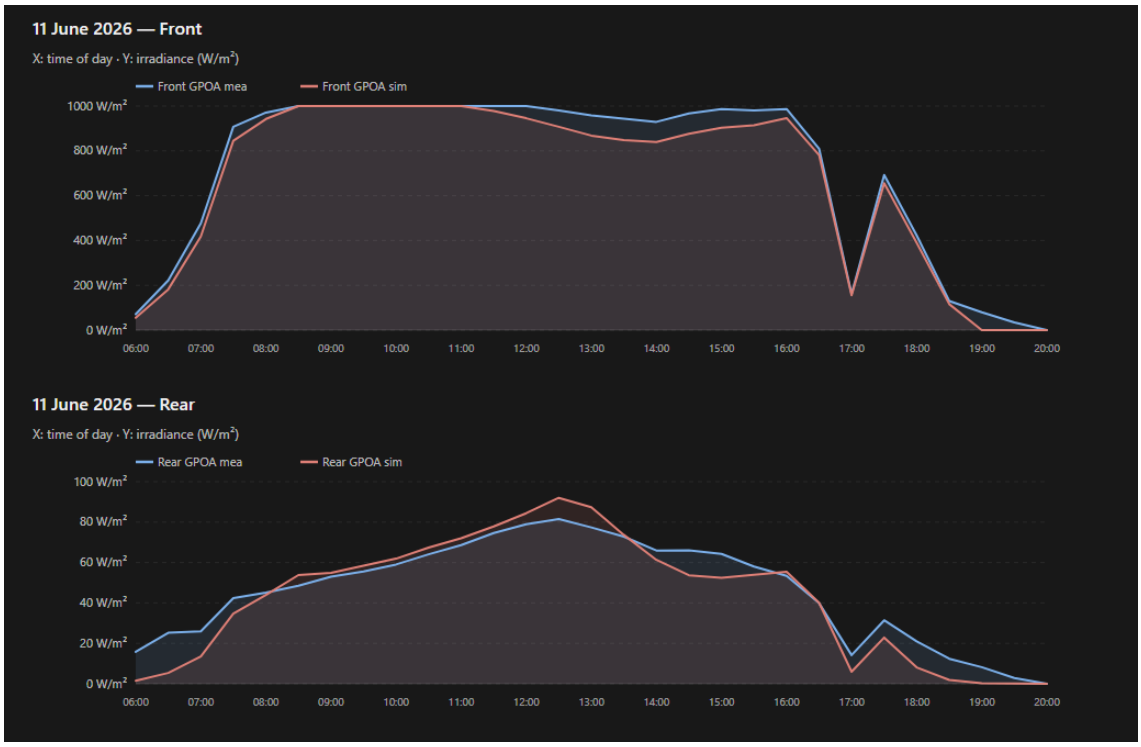


Figure 4: Comparison between measured and simulated irradiance values on the front and rear sides of the photovoltaic modules for the test day on 11 June 2026.



Figure 5: Comparison between measured and simulated irradiance values on the front and rear sides of the photovoltaic modules for the test day on 04 July 2026.

Discussion

The validation results showed a normalized Root Mean Square Error (nRMSE) of **8.2%** for the front-side irradiance and **17.4%** for the rear-side irradiance across the three test days considered. The lower error observed on the front side indicates a good agreement between simulated and measured irradiance values, confirming the model's capability to accurately reproduce the irradiance conditions directly received by the PV modules. The higher nRMSE obtained for the rear side is expected, as rear irradiance is strongly influenced by secondary reflections from the ground and surrounding objects, which are intrinsically more difficult to characterize and model accurately.

It should be noted that, prior to the validation exercise, an additional calibration step was performed for the optical parameters of the Bolzano digital model. The calibration was carried out using measurement data collected on different days from those employed for the validation presented in this section. This approach allowed the model parameters to be independently tuned while ensuring that the reported validation results were obtained against an independent dataset, thereby reducing the risk of overfitting and providing a more robust assessment of the model predictive capabilities.

Part of the discrepancy observed on the rear side can also be attributed to the simplified representation of the vegetation within the digital model. Due to modelling constraints, it is not possible to fully reproduce the actual geometry and internal structure of the plants. Previous tests performed during the model development phase showed that the geometrical assumptions adopted to represent the vegetation have a significant influence on the shape of the daily rear-side irradiance profile. In addition, the absence of branches and internal plant structures in the model reduces the amount of reflected and scattered radiation intercepted by the canopy. As a result, the simulated rear-side irradiance tends to be slightly overestimated during the central hours of the day, which could explain the systematic differences observed between simulated and measured values around solar noon.

LUSIM: 3D irradiance simulation on simplified customizable Agri-PV system

Introduction

LUSIM is a GPU-based 3D simulation tool developed by LUCISUN to assess solar irradiance in complex PV and agrivoltaic geometries. Its methodological foundations include the GPU rasterisation approach described by Robledo et al. (2019) for direct-shading calculations [8], subsequently complemented by hemispherical views and three-dimensional view factors to evaluate sky visibility and reflected irradiance in bifacial applications (Robledo et al., 2021) [9]. Within SYMBIOSYST, Deliverable D2.2 compares this approach with the Radiance-based ray-tracing frameworks used by imec and TU Delft [10]. These frameworks trace light paths through the scene, with developments including spectrally resolved optical modelling at imec and spectral skies and porous crop canopies at TU Delft. LUSIM combines GPU-based visibility calculations with view factors to assess radiation exchange across three-

dimensional surfaces. These complementary approaches provide the methodological context for the present study, which applies a simplified configurable LUSIM scene to investigate how design parameters affect irradiation received by PV modules and crops.

Task 2.4 develops specifications and tools for the early technical planning and optimisation of agrivoltaic projects, including high-level assessment of the trade-offs between PV and crops. LUCISUN contributes to this task through the configurable LUSIM scene, which uses a simplified open-field array to compare the radiation received by PV modules and crop surfaces. The assessment uses Bolzano weather and provides inputs for subsequent PV and crop modelling.

Deliverable D6.2, associated with Task 6.3, describes access to the demonstrations and operation of the interface. The present contribution examines how configurable inputs generate the scene and how changes in those inputs affect irradiation and computation time. The Bolzano location supplies coordinates and weather for the generic geometry; it does not load the physical demonstrator. Users can vary the system parameters and compare the resulting radiation distribution on PV modules and crops.

The assessment addresses four questions:

• How do backtracking and tracker spacing change crop, PV-front and PV-rear irradiation over the year and on days with different sky conditions?

• How do tracker height, crop size and count, module selection, ground albedo and rotation limit affect received irradiation?

• How do computation settings and representative-object reuse influence the results and recorded runtime?

• Which outputs can support crop modelling, and what limits must accompany their use?

Methodology

Baseline and fixed parameters

B01 defines the reference configuration. A variant named “Baseline” inside a batch denotes that batch’s first setting; it does not necessarily reproduce B01. Table 3 records the fixed B01 inputs and their physical interpretation.

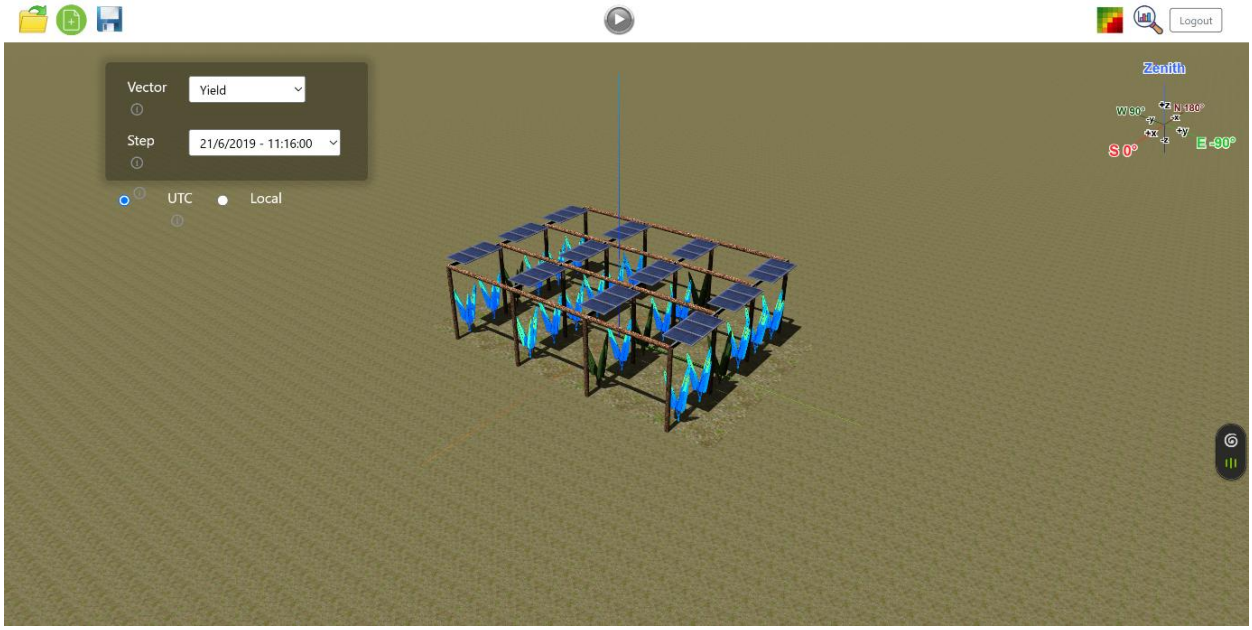


Figure 6: Generic configurable agrivoltaic scene. Illustration of the simplified array and crop objects.

Parameter	B01 value
Location	Bolzano; 46.3807° N, 11.287° E; Europe/Rome
Weather and horizon	PVGIS TMY; flat horizon
Tracker tables	3 N–S × 4 E–W = 12 independently rotating tables
PV module	Type 2 Standard_Poly60; monofacial polycrystalline
Modules	3 per table; 36 modules in total; one string per table
Module arrangement	One module deep in portrait; short side along the tracker axis; 25 mm gaps
Orientation	N–S tracker axes; azimuth input 0°
E–W pitch	5 m, centre to centre between tracker axes
Tracker height	4.7 m to the module plane at 0° tilt; rotation axis 4.55 m
Tracking	Conventional sun following; no backtracking; Max rotation limit ±50°
Crops	Model 2; 2 per table; 24 objects; height 3 m
Crop material	Fixed grass; nominal albedo 0.14
Ground material	Plowfield; nominal albedo 0.20

Parameter	B01 value
Complexity	PV high and crops high; nominal spacing 0.25 m for both
Calculation period	365 days; nominal 60-minute daylight steps; 4,400 exported steps

Table 3: Baseline Configuration

Configurable interface and model catalogue

The early-design interface provides a fixed catalogue of poles, horizontal beams, ground tiles, two crop models and two PV modules. Each model has OBJ geometry and MTL display materials; the PV models also have PVM records containing their simulation properties. Users select these built-in objects and vary the scene parameters through the input panel.

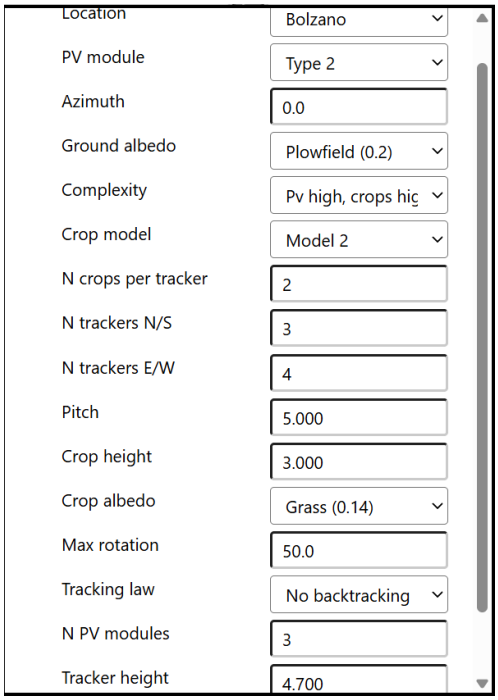


Figure 7: Configurable inputs in LUSIM. The panel shows the B01 settings, including Type 2 modules, Crop Model 2, 5 m pitch and 4.7 m tracker height

The internal LUSIM interface also provides an OBJ import and material-assignment menu, illustrated below. This menu is hidden for the SYMBIOSYST early-design role. The present assessment therefore concerns scenes generated from the fixed catalogue and does not assess arbitrary OBJ import or external remeshing.

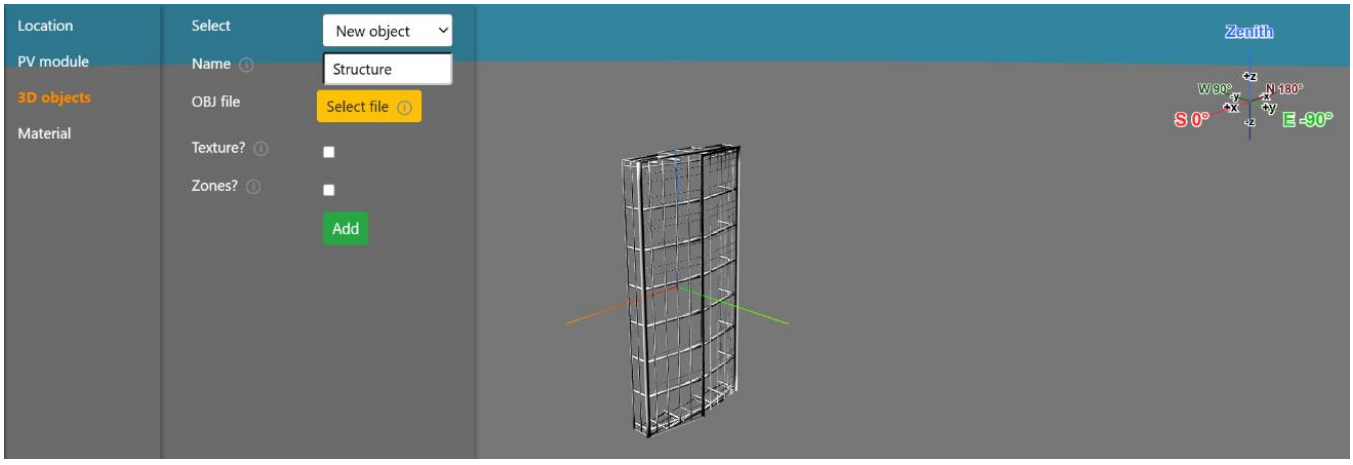


Figure 8: OBJ import menu in the internal LUSIM interface. This menu provides context for the model catalogue and is not available in the configurable early-design interface.

Scene generation and coupled parameter changes

The scene inputs have the geometric effects listed in Table 4. OBJ coordinates are used directly in metres, with Z upward and no unit conversion. Module count changes table length; pitch sets the distance between tracker axes; crop height scales the whole crop object. These coupled changes are retained when interpreting the comparisons.

All tables use the selected tracking law and the same symmetric rotation limit. The study keeps the number of tables and modules small to limit computation. The reported mean irradiation refers to each receiving surface, not to a common area of cultivated land.

The case matrix records the selected models, optical materials and tracking settings. All tables follow the same selected law, with a symmetric maximum rotation of ±50° except for B09, which uses ±60°.

Input	Effect in the scene
Pitch	Changes the E–W spacing between tracker axes. Crop positions follow the tables without changing crop scale.
Modules per table	Changes table length along the N–S axis. Modules are adjacent with 25 mm gaps and remain one module deep.
Crop count	Places the requested number of crop objects below each table. Increasing count can create canopy overlap.
Crop height	Scales the whole object by crop height / 4.2512. Width, depth and surface area change with height.
Tracker height	Sets the module plane at zero tilt. The rotation axis is 0.15 m lower; pole scaling is (height − 0.15) / 4.4.
Module selection	Changes module dimensions, table length, ground footprint and ground coverage ratio (GCR).
Ground and table repetition	Ground tiles cover the table-length × pitch footprint. Tables repeat along their axis at L + 1 m, including 0.5 m of structure at each end.
Backtracking	Uses the selected pitch and module/table width. Without backtracking, sun-following rotation is clipped at the selected angle limit.
Complexity	Sets nominal PV/crop mesh spacing: high 0.25 m, low 1 m. Representative-object reuse also contributes to the computational workload.

Table 4: Relationship between scene inputs and generated geometry

PV modules and surface properties

Property	Type 1 Mono144	Type 2 Poly60
Module image		
OBJ dimensions	1.134 × 2.285 × 0.035 m	0.992 × 1.650 × 0.040 m
Rectangular front area	2.591 m²	1.637 m²
Technology	Monocrystalline; half-cut; bifacial	Polycrystalline; monofacial
Nominal peak power	545 W	260 W
Bifaciality factor	0.7	Monofacial
Surface optics	Opaque; albedo 0.05; glossy BRDF	Opaque; albedo 0.05; glossy BRDF
Original OBJ mesh	160 vertices; 196 triangular faces	160 vertices; 196 triangular faces
GCR at 5 m pitch	0.457	0.330

Table 5: Built-in PV module properties

Table 5 presents the two module options, including their appearance, dimensions and declared technology. The PVM file were utilized to define cell positions and normals, cell layout, bypass-diode groups, bifaciality and nominal peak power of the PV modules. The simulation assigns both modules the opaque Default_PVmodules material, with albedo 0.05 and a glossy bidirectional reflectance distribution function (BRDF).

Changing module type also changes module area, table length, the represented ground footprint and cross-axis ground coverage ratio (GCR). For example, at 5 m pitch, GCR is 0.457 for PV module Type 1 and 0.330 for PV module Type 2.

Surface sampling and spatial averaging

The two crop models provide simplified receiving surfaces below the tracker tables. Their shapes produce different surface orientations and obstruction patterns. The images below illustrate those geometries; they do not establish crop species or growth characteristics.

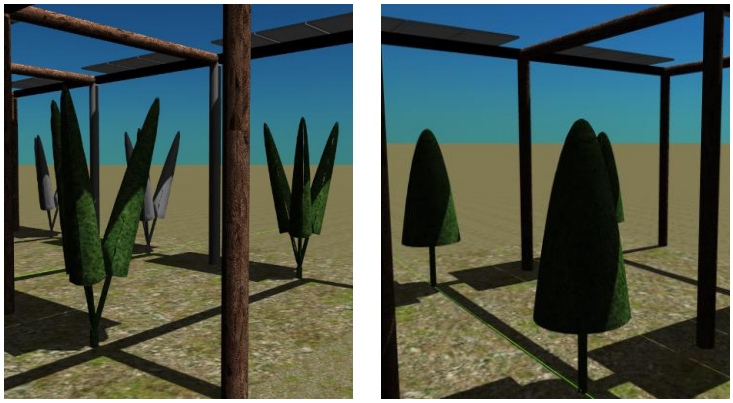


Figure 9: Simplified crop geometries. Left: the branched geometry shown for Model 2. Right: the tapered geometry shown for Model 1. The object meshes determine receiving surfaces and self-obstruction.

The catalogue crop geometries contain 659 vertices and 999 triangles for crop model 1, and 1,285 vertices and 1,500 triangles for crop model 2. These asset counts describe the source geometry, not verified receptor counts for each complexity setting. Each crop has one zone covering the complete object. The high/low settings and the remaining sampling check are described below.

For a crop surface, each triangle uses the mean irradiance of its three vertices, weighted by triangle area. The resulting object mean is:

$$\bar{G}crop(t) = \Sigma_j A_j [G_{j,1}(t) + G_{j,2}(t) + G_{j,3}(t)] / (3 \Sigma_j A_j).$$

Mesh complexity and PV sampling

High and low complexity settings specify nominal vertex spacings of 0.25 m and 1 m, respectively, for the selected PV or crop surface. Figure 10 illustrates the change in PV triangulation, including an intermediate setting not assessed here. The spacing describes mesh resolution, while the triangular remeshing does not imply an exactly uniform Cartesian grid, but still an equi distant point between each vertices.

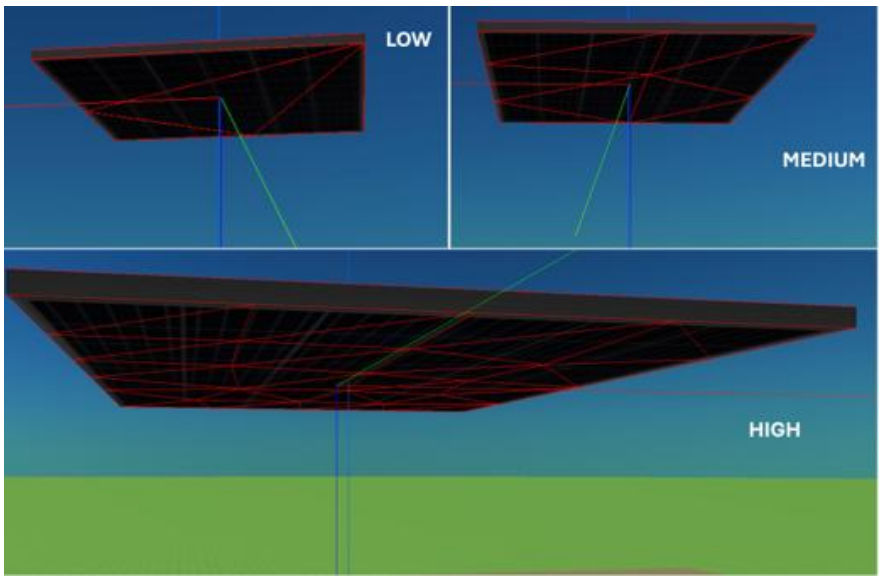


Figure 10: PV mesh complexity. Supplied illustration of low, medium and high PV triangulation. The assessed low and high settings use nominal vertex spacings of 1 m and 0.25 m. The medium setting is shown for context and is not part of the reported comparison.

PV direct shading uses a regular 5 × 5 sampling grid per cell and is calculated for every tracker. Diffuse and reflected irradiation use representative trackers and crops. B01 uses three PV representatives and five crop representatives; the remaining targets copy the nearest representative.

The assessment uses the Bolzano PVGIS typical meteorological year (TMY), the default weather input in LUSIM. A common TMY provides a consistent seasonal weather sequence for comparing designs, without making one particular observed year the basis of the comparison. It represents typical conditions rather than extreme weather or interannual variability.

Weather values use an instantaneous time convention, with any source irradiance-time offset considered and recorded in the input workflow. LUSIM uses beam-normal irradiance, isotropic diffuse irradiance and circumsolar normal irradiance. The 365-day simulation uses daylight steps centred on solar noon, so clock times need not fall on whole hours. The exported results are a selectable UTC or local time and use 2022 as a reference-year label.

The Hay–Davies treatment represents diffuse sky radiation as an isotropic background and a circumsolar component concentrated around the sun in LUSIM[11]. It uses the direct and diffuse weather inputs to describe the angular distribution of diffuse radiation and its contribution to an inclined surface; it does not itself derive direct and diffuse weather data from GHI. LUSIM then applies the scene geometry and visibility calculations to the receiving surfaces. This distinction matters when interpreting the case results, where a change in total irradiation can combine direct shading, diffuse-sky access and reflected-light contribution.

The GPU calculation uses 12 representative days, one per month, for direct shading at 60-minute intervals. Beam albedo uses those days at 120-minute intervals. Sky and diffuse-albedo view factors are evaluated at five tracker angles. Interpolation transfers these quantities onto the annual simulation steps. Thus, hourly annual output does not imply an independent GPU calculation at every hour.

A view factor describes the geometric coupling between a receiving surface and the visible sky or other surfaces [13]. It varies with receptor position, surface orientation and tracker angle. Weather changes the radiation available along those paths, rather than the geometric view factor itself. The explanations below use exported radiation components to identify plausible mechanisms; they do not claim to resolve individual light paths where tracker-angle histories or reflecting-surface contributions were not exported.

Each exported irradiance sample G_t in W/m² receives the documented nominal one-hour weight. Annual or monthly irradiation is calculated as:

$$H = \Sigma_t G_t \times 1\,h / 1{,}000, in\ kWh/m^2$$

Overnight gaps are not integrated as additional time intervals. Monthly mean daily irradiation is the monthly total divided by the number of calendar days in that month.

Spatial means and comparison indicators

Crop scene means are reconstructed using the number of crop instances assigned to each source. B01 and B07-b use weights of 2, 6, 8, 6 and 2 for their five representatives, summing to 24 objects. Because each case uses identical crop objects at a common scale, equal instance weighting reproduces area weighting across objects. PV scene means average the 12 equal-module-count strings. Crop albedo terms are disabled and zero in all analysed exports.

Relative changes are calculated as:

$$100 \times (Hcase / Hreference - 1)$$

Crop-surface, PV-front and PV-rear irradiation remain separate indicators. Rear irradiation on a monofacial module describes incident radiation and does not represent rear electrical production. Electrical power, crop yield and land-normalised energy yield are not calculated in this assessment.

Configuration matrix

The study comprises B01–B13 and the B07-b module variant. B03, B04 and B05 are batch simulations. Comparisons use the reference indicated below, preserving the coupled changes in geometry described above.

Case	Configuration change	Reference
B01	Baseline configuration; PV high / crops high	Design reference
B02	Backtracking enabled at 5 m pitch	B01
B03	Pitch 6, 9 and 12 m; backtracking enabled	Within B03; 6 m

Case	Configuration change	Reference
B04	Tracker height 4.1, 4.25 and 5.25 m; 36 crops; backtracking enabled	Within B04; 4.1 m
B05	Crop height: v1 = 2 m, v2 = 3 m, v3 = 4 m	Within B05; v1 at 2 m
B06	Type 1 Mono144; ground albedo 0.20; Crop Model 2	B08 for rear albedo response
B07	Crop Model 1; Type 2 Poly60; 2 crops per table	B01
B07-b	B07 with Type 1 Mono144; 2 crops per table	B07
B08	Type 1 Mono144; ground albedo 0.14	B06
B09	Symmetric maximum rotation ±60°	B01
B10	PV low (1 m) / crops high (0.25 m)	B01
B11	PV high (0.25 m) / crops low (1 m)	B01
B12	PV low (1 m) / crops low (1 m)	B01
B13	Crop Model 1; 3 crops per table; Type 1 Mono144	B07-b

Table 6: Simulation cases and comparison references

The design study is a set of controlled sensitivity comparisons, not a complete factorial experiment. In particular, the pitch batch uses backtracking at every pitch and cannot by itself quantify a pitch-by-tracking interaction.

Representative days and monthly profiles

Daily examples are selected from weather alone, independently of the simulated case responses. For each of January, March, June and October, the clear-sky day has the highest horizontal direct fraction among days at or above the monthly median GHI. The overcast day has a direct fraction no greater than 5%, with daily GHI closest to the median of those diffuse-day candidates.

The horizontal direct fraction is calculated from:

$$\Sigma\, BNI \times sin(solar\ elevation) \,/\, \Sigma\, GHI$$

The terms “clear-sky day” and “overcast day” identify irradiance-based selections; cloud observations are not available. It should be noted again that the selected dates refer to the TMY sequence rather than confirmed historical weather on those dates.

Month	Clear-sky day	Direct fraction	Overcast day	Direct fraction
January	21 January	81.9%	4 January	0.0%
March	31 March	77.2%	4 March	2.7%
June	23 June	75.4%	16 June	0.0%
October	20 October	71.3%	15 October	0.0%

Table 7: Days selected for detailed comparison

The same dates are used for every case comparison. Daily plots show nominal hourly samples in local time. Monthly mean diurnal profiles align each day's maximum-elevation sample with hour 12 and average across all calendar days, treating nighttime irradiance as zero. This separates seasonal mean behaviour from individual weather-day examples.

Recorded computation time

The total elapsed computation times were recorded on the reference Windows 11 computer with an Intel Core i7-11370H processor, 4 cores and 8 logical processors, 16 GB RAM, and reported NVIDIA GeForce MX450 at each run. Individual runs and multi-variant batches are reported separately under assumed comparable operating condition where each timing is a single observation. These observations do not establish performance on other hardware or scaling to larger arrays, however it is deemed a standard-level benchmark for a widely used hardware specifications in the industry.

Results

Annual irradiation

Table 8 presents annual irradiation per square metre of crop surface, PV front or PV rear. Crop values represent the scene average, with each simulated crop representative weighted by the number of crop instances it represents. PV values are averaged across the 12 strings. Because these quantities refer to different receiving surfaces, they cannot be summed to obtain an energy balance per unit land area.

Each case is compared with its specified reference to assess how the parameter change affects light availability for PV modules and crops. Annual totals describe the overall radiation resource, while monthly averages show how the response varies throughout the year. Comparisons using the same clear-sky day and overcast day days help identify the influence of direct shading and effects that remain under predominantly diffuse light. In combination, these results support the comparison of agrivoltaic design where additional electrical and crop modelling is needed to translate irradiation into electricity generation and crop performance, which will be further elaborated in D2.5 and D2.3 respectively.

Case	Variant	Crop surface	PV front	PV rear
B01	Baseline (Monofacial Modules)	296.93	1,466.12	188.94
B02	Backtracking on	300.97	1,467.53	163.81
B03	Pitch 6 m	288.62	1,466.10	143.59
B03	Pitch 9 m	293.36	1,466.35	145.49
B03	Pitch 12 m	305.83	1,467.15	151.18
B04	Height 4.1 m	256.34	1,462.85	138.83
B04	Height 4.25 m	267.01	1,463.49	143.55
B04	Height 5.25 m	279.95	1,464.39	149.90
B05	Crop 2 m (v1)	316.05	1,467.50	167.39
B05	Crop 3 m (v2)	292.70	1,466.88	160.68
B05	Crop 4 m (v3)	263.83	1,465.63	149.60
B06	Type 1 Bifacial Modules	275.77	1,443.73	147.79
B07	Crop type 1 Monofacial Modules	346.78	1,465.97	147.42
B07-b	Crop type 1 Bifacial Modules	326.80	1,443.73	151.10
B08	Ground Albedo = 0.14 (Grass)	270.57	1,441.39	124.93
B09	Max Rotation 60°	254.59	1,455.10	146.38
B10	Complexity Mesh PV low crops high	288.07	1,460.56	147.34
B11	Complexity Mesh PV high, crops low	288.07	1,461.25	175.91

Case	Variant	Crop surface	PV front	PV rear
B12	Complexity Mesh PV low, crops low	266.07	1,458.11	118.59
B13	Increase number of crops from 2 per row to 3	318.75	1,443.80	148.29

Table 8: Annual irradiation in kWh/m²/year

B01 — Baseline light distribution

The baseline establishes the radiation environment against which the controlled changes are assessed. It contains 12 independent tracker tables arranged as 3 N/S × 4 E/W, with three Type 2 Poly60 modules and two Crop Model 2 objects per table: 36 modules and 24 crops in total. The N–S tracker axes use azimuth 0°, 5 m pitch and a 4.7 m module-plane height at zero tilt, with the rotation axis 0.15 m lower. Crops are 3 m high; ground and crop albedos are 0.20 and 0.14. All tables follow the sun without backtracking, subject to a symmetric ±50° limit, using high PV and crop complexity.

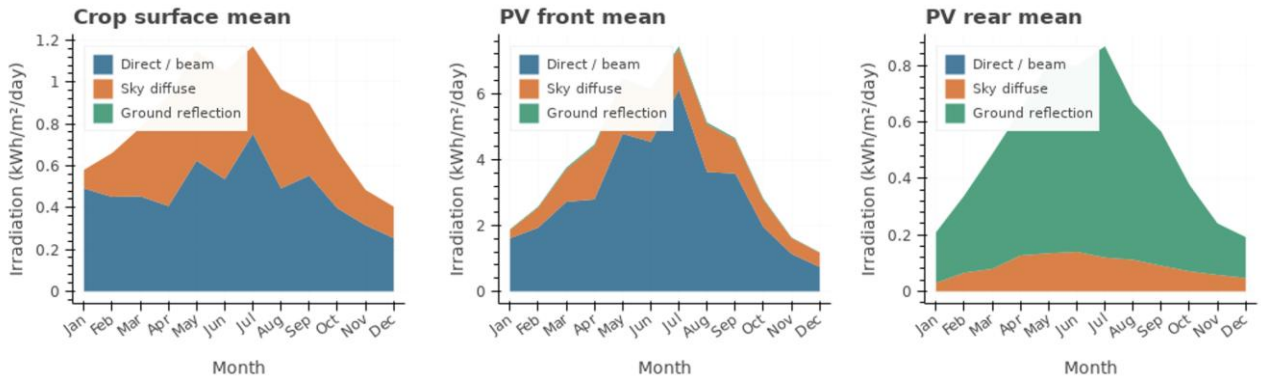


Figure 11: Baseline monthly radiation components. Each panel uses its own vertical scale. Values are monthly mean daily irradiation.

Annual irradiation averages 296.93 kWh/m² across crop surfaces, 1,466.12 kWh/m² across PV fronts and 188.94 kWh/m² across PV rears. Figure 11 illustrates how the balance of radiation components differs between these receiving surfaces. For crops, the exported beam component contributes 58.7% of annual irradiation, while sky diffuse radiation accounts for the remaining 41.3%. Assessing crop light availability therefore requires consideration of both direct shading and access to the diffuse sky as shadow duration alone does not capture the full radiation resource.

PV front-side receive an average of 73.9% of their irradiation from the beam component, 25.0% from sky diffuse light and 1.1% from reflected light. The rear-side balance is different, where 82.7% comes from the reflected component and 17.3% from sky diffuse light. The front therefore mainly tests access to the direct solar resource, whereas the rear is especially sensitive to the visible reflecting environment and its illumination. This is consistent with the geometric role of view factors in bifacial and tracker modelling notion in research [13].

Poly60, the type of panel used in this case is monofacial, so its rear irradiation is an optical diagnostic rather than rear electrical production. In the agrivoltaic assessment, the crop result describes the mean light received per unit modelled crop surface.

B02 — Backtracking and the annual radiation balance

Backtracking is a control strategy for PV trackers that reduces shading between tracker rows by adjusting their rotation away from conventional sun following when required by the array geometry [12]. For PV performance, this involves a trade-off between reduced row shading and a less favourable angle of incidence. In an agrivoltaic system, these adjustments also shift shadows beneath the tables and alter the crop surfaces' exposure to the sky and surrounding reflective surfaces. B02 is therefore compared with B01 to assess changes in crop, PV-front and PV-rear irradiation under the same geometry and weather conditions.

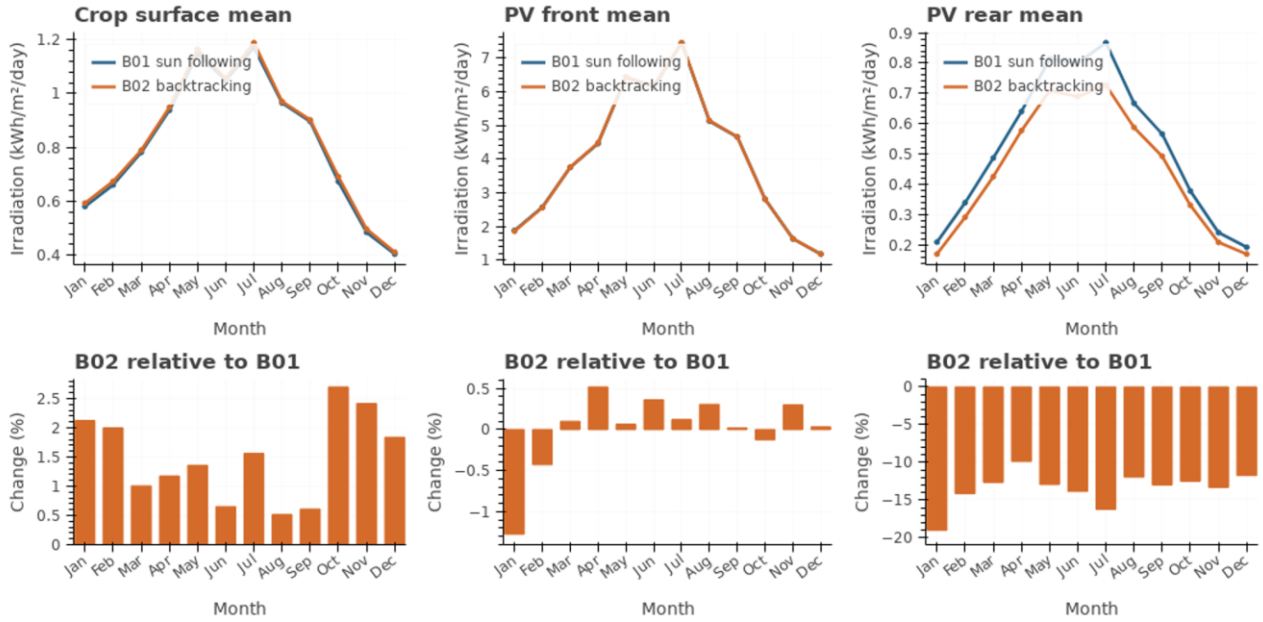


Figure 12: Monthly backtracking comparison. B02 relative to B01. Upper panels show mean daily irradiation; lower panels show monthly percentage changes.

Enabling backtracking produces a small annual increase in irradiation on both crops and PV fronts: 4.05 kWh/m² (+1.36%) and 1.40 kWh/m² (+0.096%), respectively. Rear irradiation, however, decreases by 25.13 kWh/m² (−13.30%). The almost unchanged front total masks a redistribution between radiation components. A 6.28 kWh/m² increase in sky diffuse irradiation offsets reductions of 3.74 kWh/m² in beam irradiation and 1.13 kWh/m² in reflected light. Backtracking therefore changes how the module receives light, even though its total annual front irradiation remains nearly the same.

For crops, the result indicates a modest improvement in annual light availability per unit crop surface under the tested configuration. The more pronounced rear decrease illustrates that a tracking strategy intended to reduce shading on PV fronts can also reduce the light reaching their undersides. Since B01 and B02 use monofacial modules, this rear decrease does not translate into a loss of bifacial electricity generation. Assessing its implications for bifacial PV would require an equivalent comparison using bifacial modules, followed by electrical modelling.

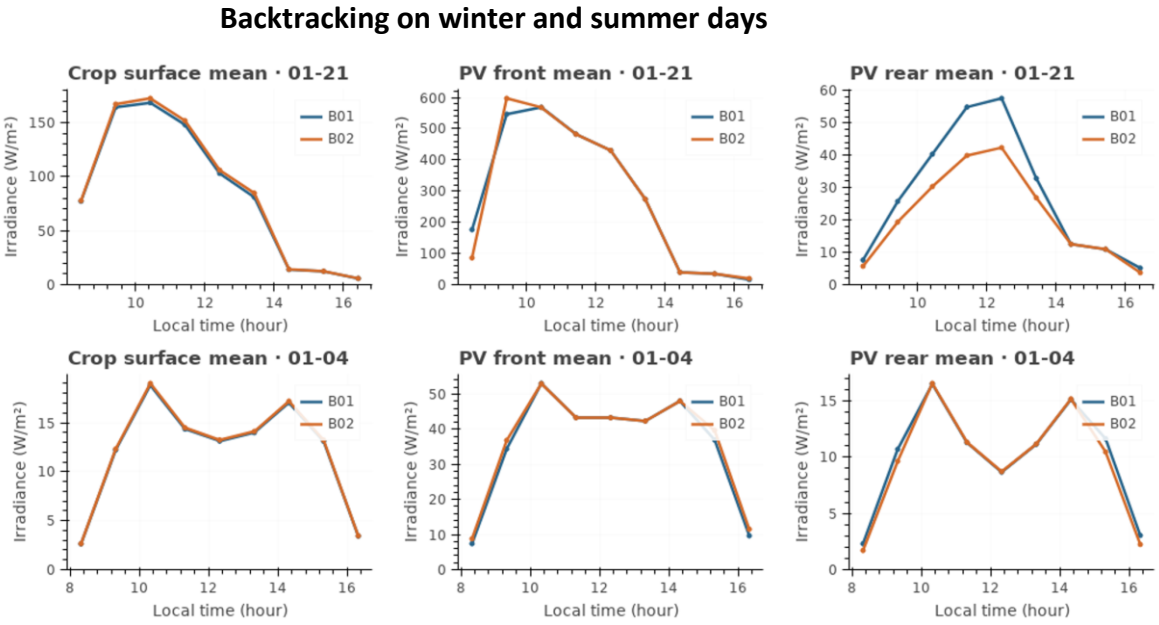


Figure 13: January backtracking examples. Upper row: clear-sky day 21 January. Lower row: overcast day 4 January.

The January examples show how the response to backtracking varies with sky conditions. On the clear-sky day of 21 January, crop irradiation increases by 2.35%, while PV-front and rear irradiation decrease by 1.45% and 22.57%, respectively. On the overcast day of 4 January, both crops and PV fronts receive more irradiation (+0.88% and +2.61%), while the rear decrease is smaller (−3.79%). The contrasting front responses highlight the importance of tracker orientation and access to diffuse sky radiation, alongside the reduction of direct shading. Crops receive a modest increase on both days, although its agricultural relevance depends on whether cultivation takes place during winter and on the crop's light requirements.

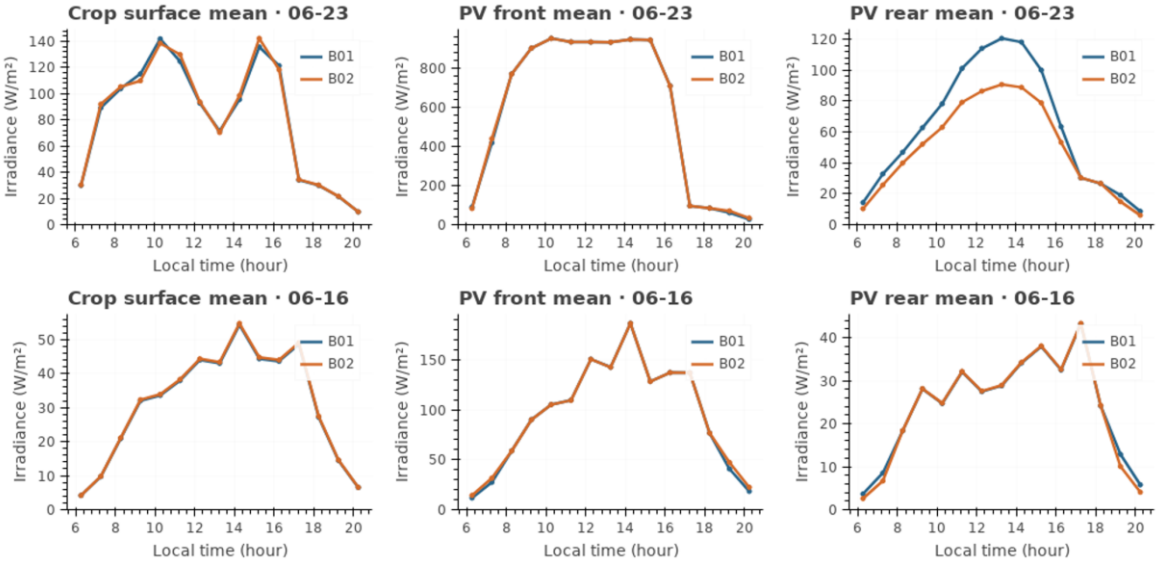


Figure 14: June backtracking examples. Upper row: clear-sky day 23 June. Lower row: overcast day 16 June.

On clear-sky day 23 June, crop and front irradiation increase by 0.68% and 0.32%, while rear irradiation decreases by 20.35%. On overcast day 16 June, the changes are +0.86%, +1.19% and −1.74%. The larger clear-sky day reduction is consistent with a change in reflected direct sunlight, although the export does

not separate reflected beam and diffuse radiation. The small crop increases describe light availability; their agronomic interpretation requires the daily profile and crop growth stage.

Backtracking during transition seasons

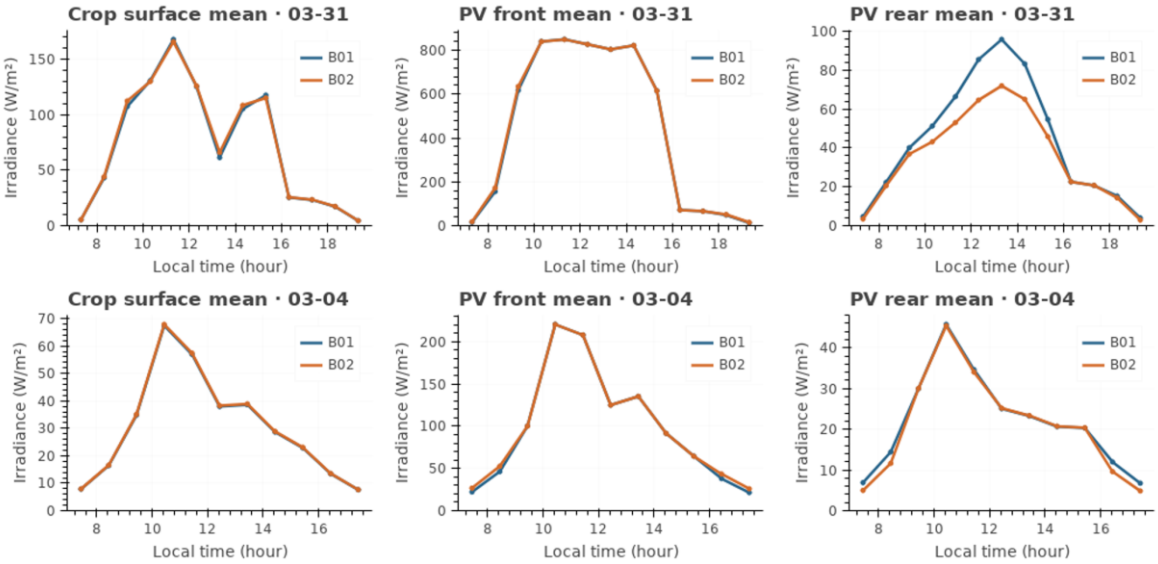


Figure 15: March backtracking examples. Upper row: clear-sky day 31 March. Lower row: overcast day 4 March.

Figure 15 shows how backtracking affects crop and PV irradiation under different sky conditions. Compared with sun following without backtracking (B01), B02 increases daily crop and PV-front irradiation by 1.05% and 0.71% on the clear-sky example of 31 March, while rear irradiation decreases by 17.89%. On the overcast example of 4 March, the corresponding changes are +0.78%, +1.92% and −3.98%. Backtracking therefore provides a small crop-light increase on both days, but its effect on the PV radiation balance differs considerably. The positive front-side response on 31 March contrasts with the reduction observed in the January clear-sky example, highlighting the need to assess seasonal behaviour before drawing conclusions about annual benefits. For crops, the relevance of the additional March irradiation depends on whether it coincides with active growth and periods of light limitation.

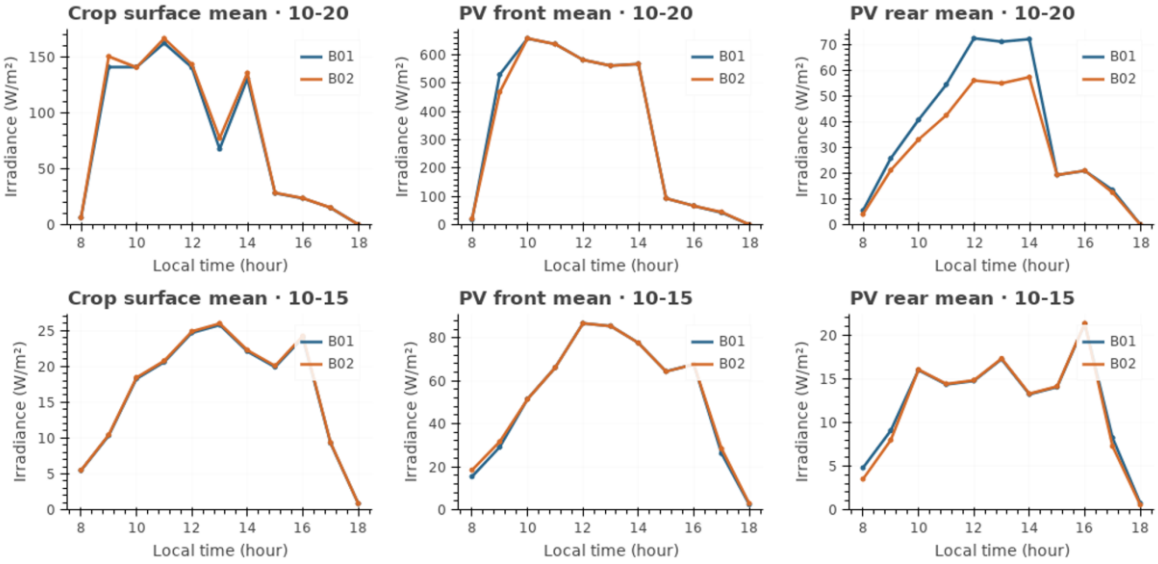


Figure 16: October backtracking examples. Upper row: clear-sky day 20 October. Lower row: overcast day 15 October.

On clear-sky day 20 October, crop irradiation increases by 3.67%, while front and rear irradiation decrease by 1.48% and 18.62%. On overcast day 15 October, crops and fronts increase by 0.83% and 1.42%, and rears decrease by 2.34%. The clear-sky day example therefore identifies a crop-light benefit alongside lower front irradiation. This is relevant to agrivoltaic assessment even though the tracking law is not optimised for crop demand. Annual totals combine these contrasting seasonal responses.

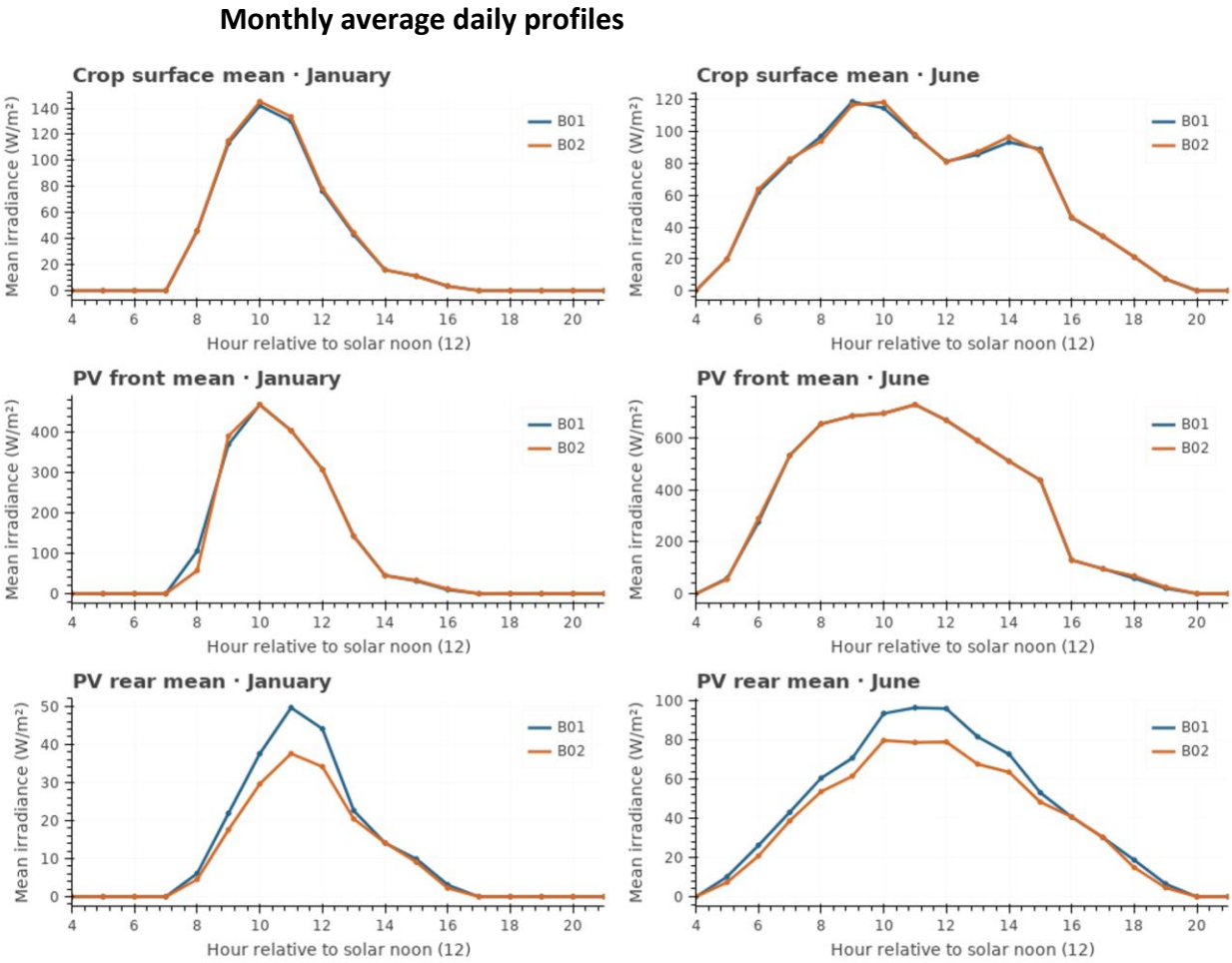


Figure 17: Mean January and June daily profiles. All days in each month are included. Hour 12 denotes the highest-elevation sample of each day.

Month	Crop surface	PV front	PV rear
January	+2.13%	-1.27%	-19.01%
March	+1.01%	+0.10%	-12.65%
April	+1.18%	+0.52%	-9.87%
June	+0.65%	+0.36%	-13.85%
August	+0.51%	+0.31%	-11.95%
October	+2.70%	-0.12%	-12.50%

Table 9: Monthly backtracking changes relative to B01

Monthly averaging confirms that the annual front response masks seasonal cancellation. PV-front changes range from −1.27% in January to +0.52% in April, with +0.36% in June. Crop irradiation increases in every month, from +0.51% in August to +2.70% in October; the changes are +2.13% in January, +1.01% in March, +1.18% in April and +0.65% in June. Rear irradiation decreases in every month.

For PV assessment, the monthly and mean daily profiles show when small annual differences arise and whether they coincide with high-resource periods. For agrivoltaics, they allow the light response to be matched to cultivation and growth stages. A larger percentage increase in a low-light month does not necessarily provide a larger absolute radiation increment. No crop-specific preference between the tracking laws is established because crop phenology and physiological response are outside this optical comparison.

B03 — Tracker pitch and land-use implications

The pitch batch tests whether greater separation between tracker rows improves crop access to light and the rear-side radiation resource. Its PV context is the balance between irradiation per module and installed capacity per unit land; its agrivoltaic context is the distribution of light within the planting arrangement. This distinction underpins agrivoltaic land-use assessment [14]. All three pitches, 6, 9 and 12 m, use backtracking, and crops remain directly beneath the rows.

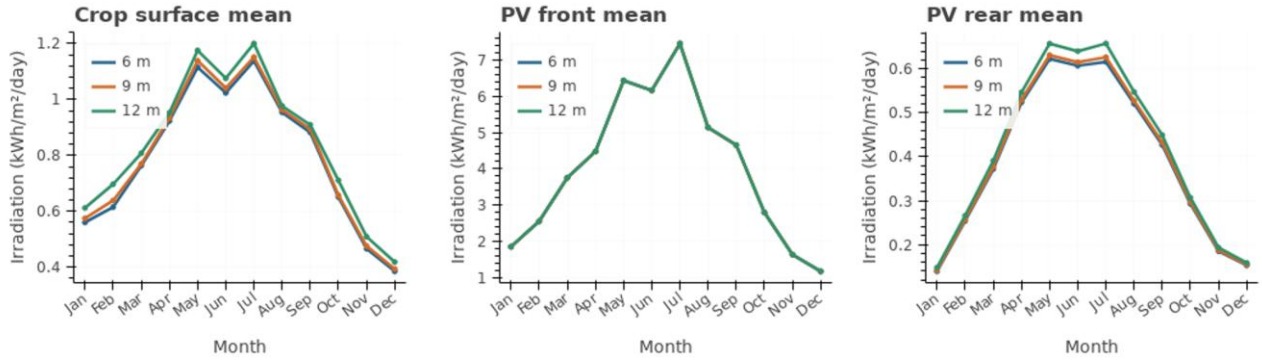


Figure 18: Pitch comparison with backtracking. B03 pitches of 6, 9 and 12 m.

Increasing pitch from 6 to 12 m raises annual crop irradiation from 288.62 to 305.83 kWh/m² (+5.97%) and rear irradiation by 5.29%, while front irradiation changes by only +0.071%. Crop mean daily irradiation rises from 0.560 to 0.612 kWh/m²/day in January and from 1.023 to 1.075 in June. For this array, the main optical response to wider spacing is therefore on the crop and rear surfaces, rather than the PV front.

The wider spacing changes obstruction by neighbouring rows and the illuminated surfaces visible to the receptors. The crop improvement persists on both June examples: +5.94% on clear-sky day 23 June and +3.98% on overcast day 16 June. This persistence is consistent with changes in diffuse-sky access alongside direct shading. These component-based explanations do not isolate individual light paths.

With the same number of tables, greater pitch also increases the array footprint. The reported gains per square metre of receiving surface therefore cannot establish an increase in energy or crop output per hectare. The crops move with their tracker rows without being rescaled; additional inter-row cropping is not represented. B03 supports an assessment of spacing within this planting pattern, but it does not establish an optimum pitch or isolate a pitch-by-backtracking interaction.

The coordinate columns in the B03 CSV describe the 5 m base scene. The simulated variant geometries use the specified pitches of 6, 9 and 12 m; the unchanged coordinate metadata are not used to infer variant spacing.

B04 — Tracker height and vertical separation

The tracker-height batch examines whether additional separation between modules and crops improves crop illumination and rear-side access to the surrounding radiation field. In practical agrivoltaic design, height also affects agricultural access and structural requirements, but those engineering and cost effects are not modelled here. B04 uses module-plane heights of 4.1, 4.25 and 5.25 m at zero tilt, with backtracking and 36 crop objects in every variant.

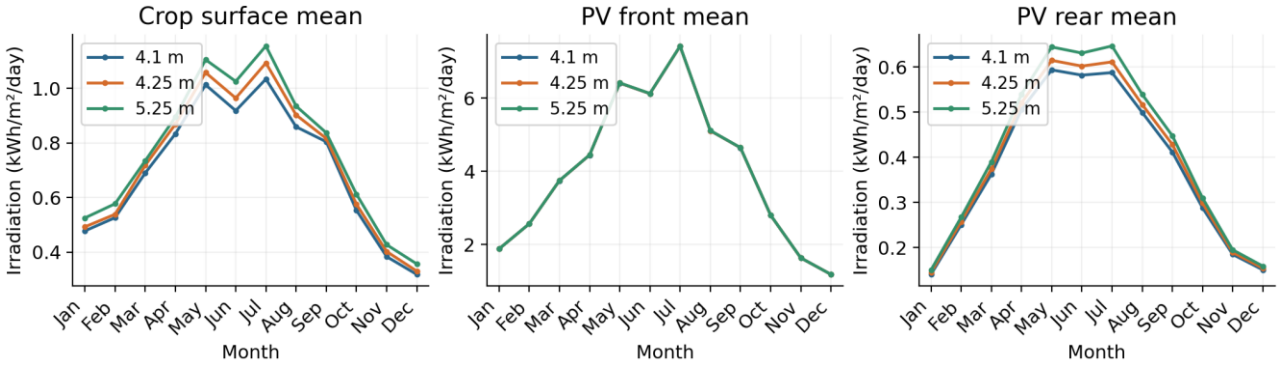


Figure 19: Tracker-height comparison. B04 heights of 4.1, 4.25 and 5.25 m, with backtracking enabled and 36 crop instances.

Annual crop irradiation increases from 256.34 to 267.01 and 279.95 kWh/m² across the three heights. Raising the tracker from 4.1 to 5.25 m increases crop irradiation by 9.21% and rear irradiation by 7.97%, while the front-side change is +0.105%. June crop mean daily irradiation increases from 0.918 to 1.025 kWh/m²/day. The additional height therefore mainly changes the light environment below and behind the modules in this configuration.

The June examples help explain the annual result. Crop irradiation increases by 15.05% on clear-sky day 23 June and by 5.82% on overcast day 16 June. The larger clear-sky day response is consistent with a stronger redistribution of direct shadows, while the diffuse-day improvement indicates that access to the sky also changes. Greater height can change which ground and crop surfaces are visible to the PV rear, providing a plausible explanation for its increased irradiation.

All assessed geometries were confirmed to have feasible crop clearance without overlap or module contact. The optical gain at greater height should therefore inform a wider design assessment of light, access and structure, rather than be interpreted as evidence that the tallest option is universally preferable.

B05 — Crop size and daily light distribution

B05 examines how the size of the crop geometry changes its own light exposure and the PV rear environment. The comparison uses v1 = 2 m, v2 = 3 m and v3 = 4 m crop height, with v1 as the reference. The input scales the whole crop uniformly, so width, depth and receiving area increase with height. This is a geometric sensitivity study of canopy size, rather than a simulation of crop growth over time.

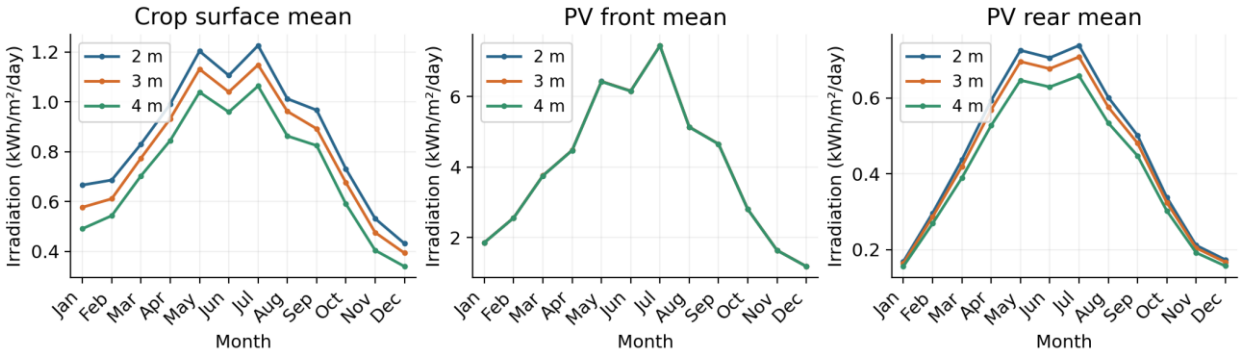


Figure 20: Crop-height comparison. B05 heights of 2, 3 and 4 m. Uniform scaling changes the whole crop geometry.

Annual crop irradiation decreases from 316.05 kWh/m² at 2 m to 292.70 at 3 m and 263.83 at 4 m. Rear irradiation also decreases, from 167.39 to 160.68 and 149.60 kWh/m²/year. The 4 m crops therefore receive 16.52% less mean irradiation per unit surface and produce a 10.63% lower rear optical resource than the 2 m crops. This ordering holds in every month and for all five crop representatives. PV-front irradiation changes much less, decreasing by 0.127%, from 1,467.50 to 1,465.63 kWh/m²/year.

Uniform scaling leaves the orientation of each corresponding crop facet unchanged, but moves the receiving surfaces relative to the modules, ground and neighbouring crops. The resulting changes in obstruction and sky access provide a plausible explanation for the lower crop-surface mean. Rear reflected irradiation falls from 138.20 to 120.42 kWh/m²/year, while its sky-diffuse contribution remains near 29.19. Larger crops can shade or obscure ground that contributes reflected light to the rear; the available component exports support this interpretation without separating ground shadowing from obstruction of the reflected-light path.

For PV design, the result shows why vegetation geometry matters to rear irradiance even when its effect on the module front is small. For agrivoltaics, a lower mean per square metre of a larger crop does not establish lower total intercepted radiation or biomass: the total represented crop surface also increases. The calculation contains no physiological adaptation, seasonal development or yield model, and therefore cannot identify a preferred crop height.

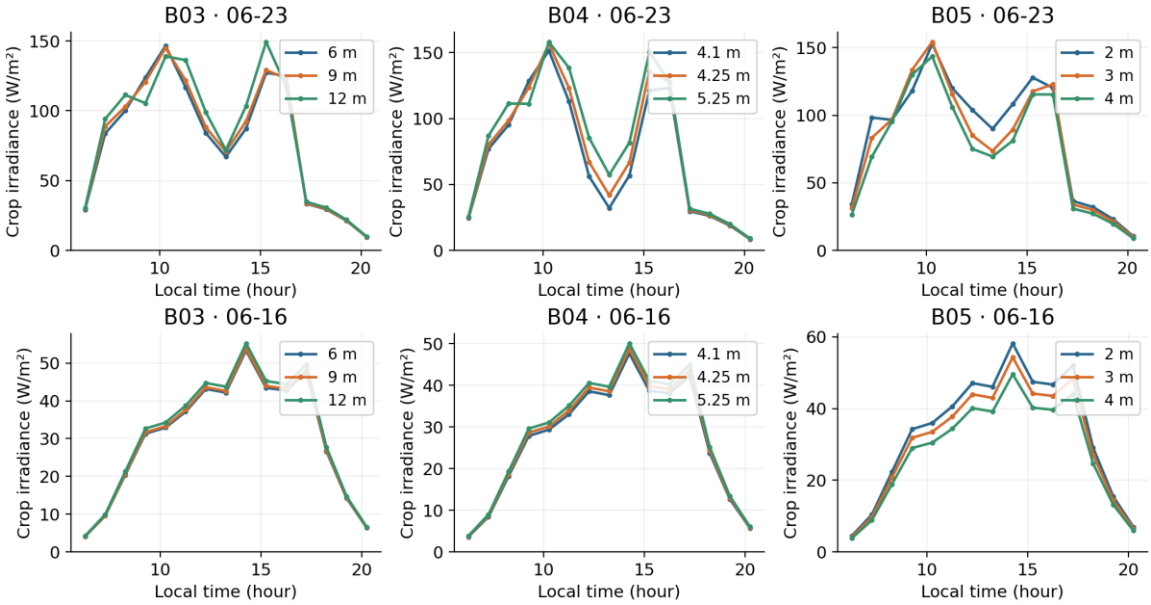


Figure 21: Geometry responses on June example days. Upper row: clear-sky day 23 June. Lower row: overcast day 16 June.

Figure 21 compares the geometry effects under the same June weather. Relative to 6 m pitch, 12 m pitch increases crop irradiation by 5.94% on 23 June and 3.98% on 16 June. Raising the B04 tracker from 4.1 to 5.25 m increases it by 15.05% and 5.82%. In B05, 4 m crops receive 12.44% and 15.12% less mean irradiation than 2 m crops on those days.

The B05 decrease on the diffuse day demonstrates that the crop-size response is not confined to direct shadows. Taken together, the batches distinguish two design actions: changing the space around a fixed crop geometry and enlarging the crop geometry within the array. Their agronomic consequences require the receiving crop model to account for both light availability and the area and structure of the canopy.

B06 and B08 — Bifacial rear resource and ground albedo

B06 introduces the larger, bifacial Type 1 Mono144 module to examine the radiation available at the rear and establish the reference for the albedo comparison. Module selection also changes physical dimensions and array geometry, so it cannot isolate the effect of bifacial conversion alone. The complete B07/B07-b pair, discussed below, provides the matched module comparison for Crop Model 1.

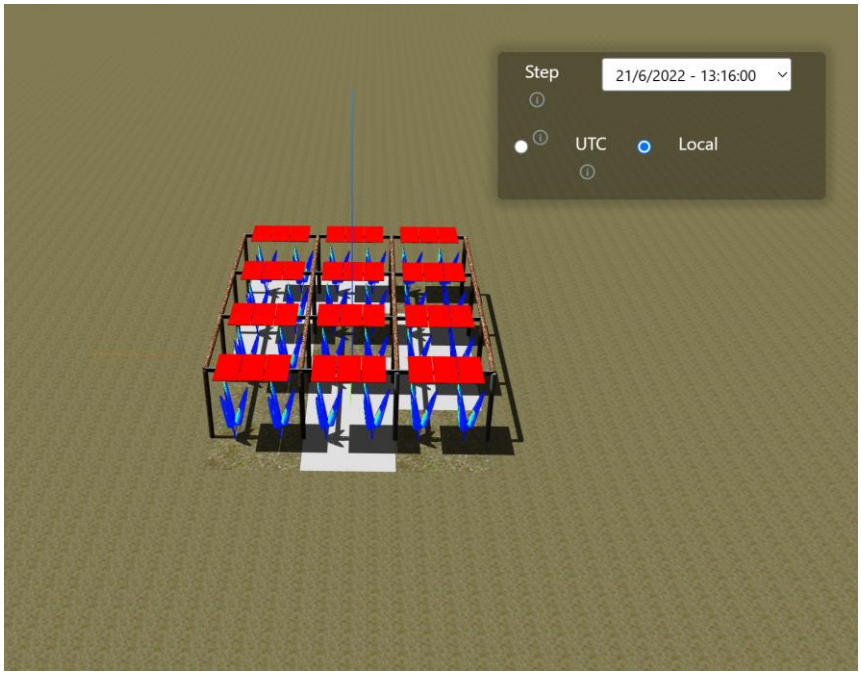


Figure 22: Type 1 module scene. Mono144 modules above Crop Model 2. The screenshot illustrates the configuration; its colours have no supplied quantitative legend.

In B06, annual rear irradiation is 147.79 kWh/m²: 32.95 from sky diffuse light and 114.83 from the reflected component. This identifies reflection as the dominant rear contribution in this scene. The result describes radiation incident on the module, not electrical energy. Bifacial electricity generation would also depend on rear response, non-uniformity, temperature and the electrical model. B06 front and crop totals remain subject to the highlighted export check accompanying Table 8.

B08 tests the effect of ground reflectance while retaining the B06 module and all other inputs. Ground albedo is the only change, from 0.20 to 0.14; crop albedo remains 0.14. Both cases use Mono144, the same weather and crop geometry, 5 m pitch, 4.7 m tracker height and sun following without backtracking at ±50°. In PV terms, this isolates a ground-treatment sensitivity of the rear resource. In agrivoltaic terms, it represents the optical effect of the selected ground reflectance, without modelling the agronomic differences between grass and ploughed soil.

Rear component	B06 albedo 0.20	B08 albedo 0.14	Change
Sky diffuse	32.95	32.92	-0.11%
Ground reflection	114.83	92.01	−19.87%
Total	147.79	124.93	−15.46%

Table 10: Albedo effect on annual rear irradiation

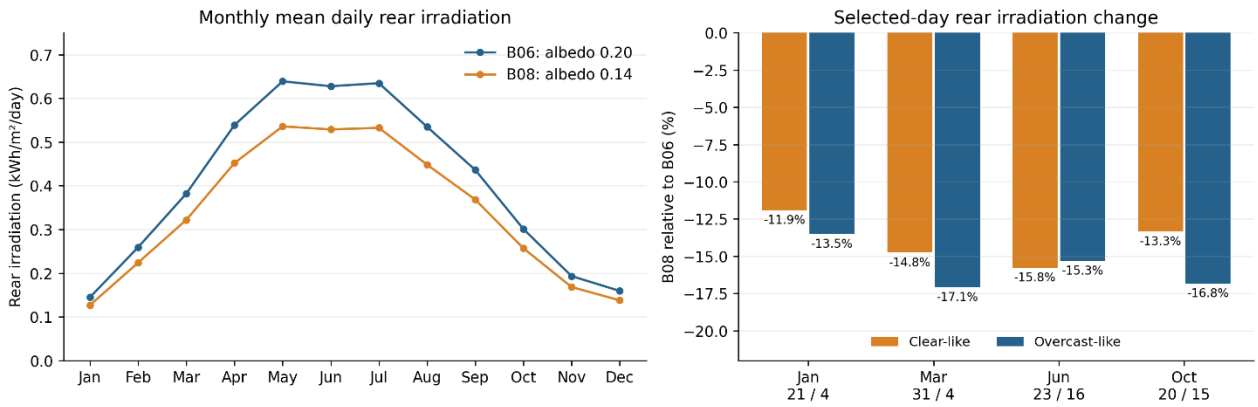


Figure 23: Seasonal and daily albedo response. Left: monthly mean daily rear irradiation. Right: percentage changes on the selected clear-sky day and overcast day days.

Annual rear irradiation falls from 147.79 kWh/m² in B06 to 124.93 kWh/m² in B08, a reduction of 22.85 kWh/m² (15.46%). This decrease is almost entirely associated with reflected radiation, which drops from 114.83 to 92.01 kWh/m² (19.87%), while the sky diffuse contribution remains nearly unchanged at approximately 32.9 kWh/m². Reflected radiation accounts for 99.85% of the rear decrease, consistent with lower ground reflectance reducing the light available to the underside of the bifacial modules.

The reduction occurs throughout the year, ranging from 12.52% in January to 16.21% in August. The selected June days show similar relative decreases: 15.78% on clear-sky day 23 June and 15.32% on overcast day 16 June. However, the absolute loss is greater on the clear-sky day, at 0.099 kWh/m² compared with 0.056 kWh/m² under overcast day conditions. Ground reflectance therefore influences rear irradiation under both conditions in these examples, although the two days alone cannot establish whether clear or overcast conditions generally produce greater sensitivity.

B07 and B09 — Crop geometry and tracker rotation range

B07 tests the influence of crop representation by replacing Crop Model 2 with Crop Model 1 while retaining Poly60 modules and two crops per table. Its agrivoltaic objective is to identify how canopy shape and receiving-surface orientation affect the reported crop light environment. Its PV objective is to establish whether this vegetation change alters rear panel production to diffuse and reflected radiation.

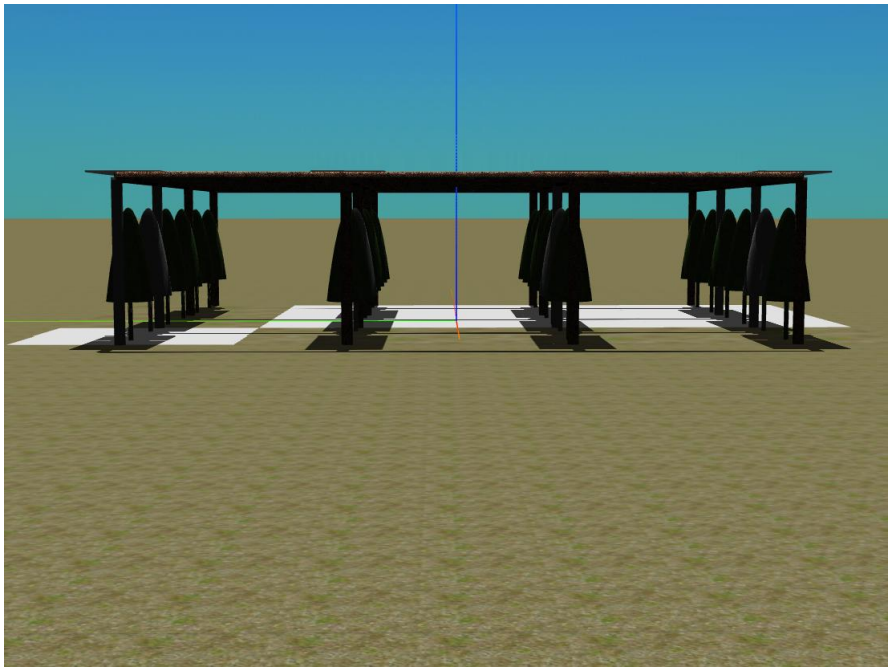


Figure 24: Crop Model 1 geometry. The wider crop crown changes the receiving surface and obstruction around the modules.

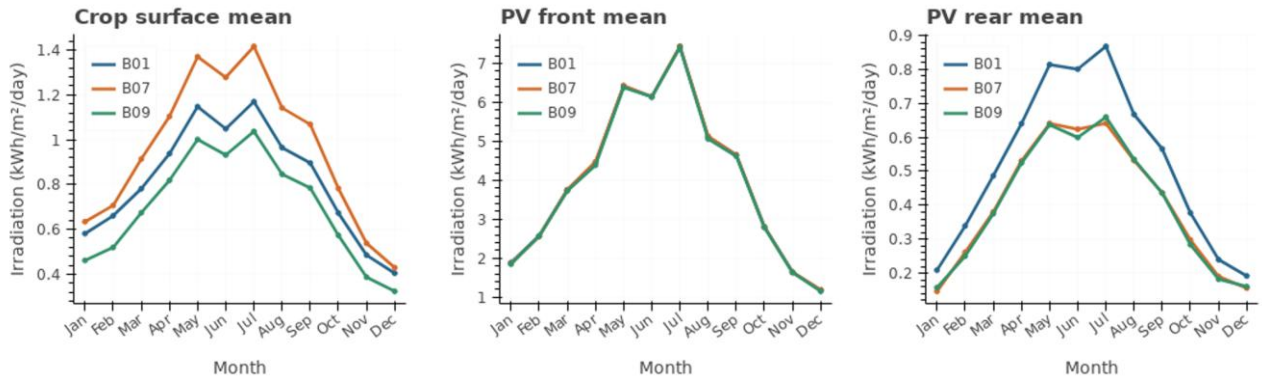


Figure 25: Monthly crop-model and rotation comparisons. B07 and B09 compared with B01.

Crop Model 1 receives 346.78 kWh/m²/year, 16.79% above B01, while PV-front irradiation is nearly unchanged (−0.010%) and rear irradiation is 21.98% lower. A higher crop-surface mean can therefore coincide with a lower rear radiation resource. Different shapes redistribute exposed facets and obstruction around the modules; they can alter the crop average and the reflecting surfaces visible from the PV rear in different directions.

This is a comparison of modelled geometry, not a ranking of crop species or their growth potential. Crop response to partial shade also involves canopy development, leaf area and radiation-use processes, as illustrated by agrivoltaic crop studies [15]. Those biological responses are not represented by switching between static OBJ models.

B09 — Maximum tracker rotation

B09 extends the symmetric sun-following limit from ±50° to ±60°, retaining the other B01 inputs. The PV objective is to assess whether the additional rotation range improves received irradiation during periods when the original limit constrains sun following. The agrivoltaic objective is to quantify the associated change in light below the trackers, where a different tilt can alter both shadow location and sky visibility.

Annual irradiation falls to 254.59 kWh/m² on crops, 1,455.10 on PV fronts and 146.38 on PV rears: changes of −14.26%, −0.75% and −22.53% relative to B01. The wider rotation range therefore does not increase annual front irradiation in this scene, and its crop and rear effects are substantially larger. Following the sun over a wider range does not by itself guarantee a higher annual optical result once row shading, diffuse light and reflected radiation are included.

Changes in incidence angle, inter-row obstruction and visible sky or ground are plausible contributors to this response. Actual tracker-angle histories were not exported, so their separate contributions cannot be verified from these results. B09 identifies a configuration-specific sensitivity that matters for both PV and crop light; it does not establish a universal optimum rotation limit or a crop-oriented tracking strategy.

B07-b — Module selection with Crop Model 1

B07-b changes the PV module in B07 from Type 2 Poly60 to Type 1 Mono144, retaining Crop Model 1 and two crops per table, or 24 crops beneath 12 tables. The remaining panel inputs are held at the B07 values. This comparison asks how a practical module selection changes both the PV radiation resource and the crop light environment.

The module types differ in size as well as cell technology, nameplate power and bifacial response. Their optical comparison must therefore be interpreted as a coupled module-and-geometry change. It cannot attribute a radiation difference to monocrystalline versus polycrystalline conversion or to the bifaciality factor alone.

Parameter	B07	B07-b
PV module	Type 2 Poly60	Type 1 Mono144
Technology	Monofacial polycrystalline	Bifacial monocrystalline
Crop count and model	2/table; Model 1	2/table; Model 1
Annual crop irradiation	346.78 kWh/m²	326.80 kWh/m²
Annual PV-front irradiation	1,465.97 kWh/m²	1,443.73 kWh/m²
Annual PV-rear irradiation	147.42 kWh/m²	151.10 kWh/m²

Table 11: B07 and B07-b module comparison

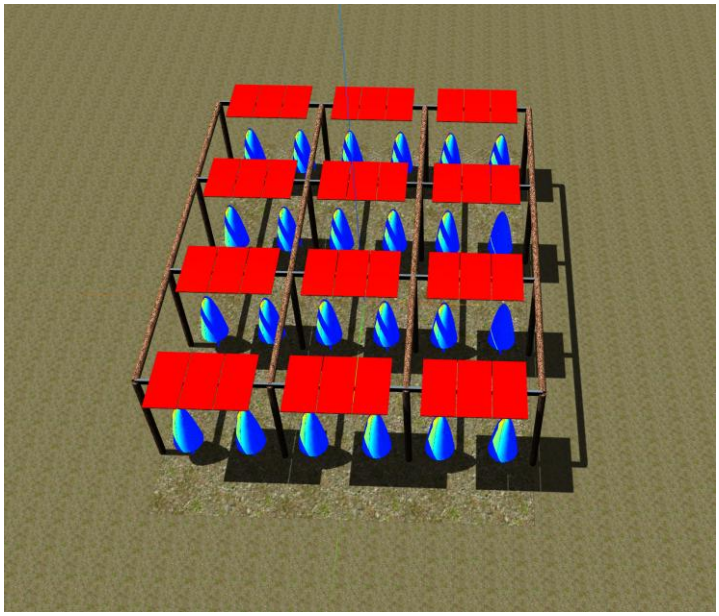


Figure 26: B07-b scene with Mono144 modules. Three modules and two crop objects per table. The image has no timestamp or quantitative colour legend.

The module change lowers annual crop irradiation by 5.76% and front irradiation by 1.52%, while rear irradiation increases by 2.49%. At unchanged pitch, Mono144's greater cross-axis length raises GCR from 0.330 to 0.457. Its greater width also changes table length and the associated crop and ground arrangement. The crop decrease is therefore relevant to the physical coverage created by module selection, rather than to an electrical material property.

The rear increase of 3.68 kWh/m²/year is dominated by an additional 3.74 kWh/m² of sky diffuse irradiation; reflected irradiation changes by only −0.064 kWh/m². The rear benefit is thus associated mainly with diffuse-sky access in this comparison. A lower front value per square metre does not establish lower electricity production because module area, nameplate power and rear electrical response also change.

For early agrivoltaic design, this pair shows that selecting a larger bifacial module can alter crop light even when table count and nominal pitch are unchanged. Module choice should therefore be carried through the scene-generation geometry before assessing crop compatibility, followed by an electrical model to determine the PV energy consequence.

Seasonal and daily module response

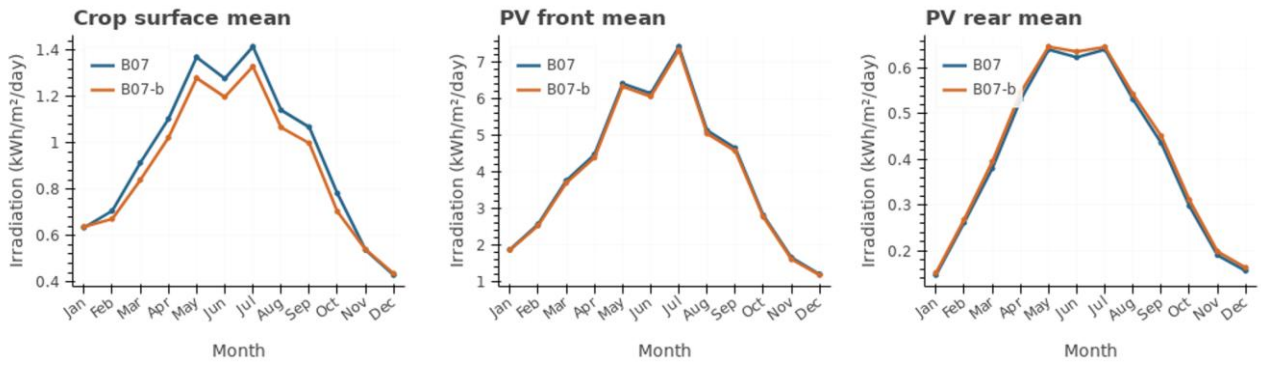


Figure 27: Monthly module-selection response. B07-b versus B07, with Crop Model 1 and two crops per table.

The crop response varies by season: +0.65% in January, −8.08% in March, −6.22% in June and −10.06% in October. Rear irradiation increases by 3.21%, 3.91%, 1.98% and 4.41% in those months. The annual crop decrease therefore does not describe every cultivation period equally. These monthly contrasts can inform a later crop-model assessment by identifying when the module geometry changes light supply, while the rear series describes the seasonal optical resource available to the bifacial module.

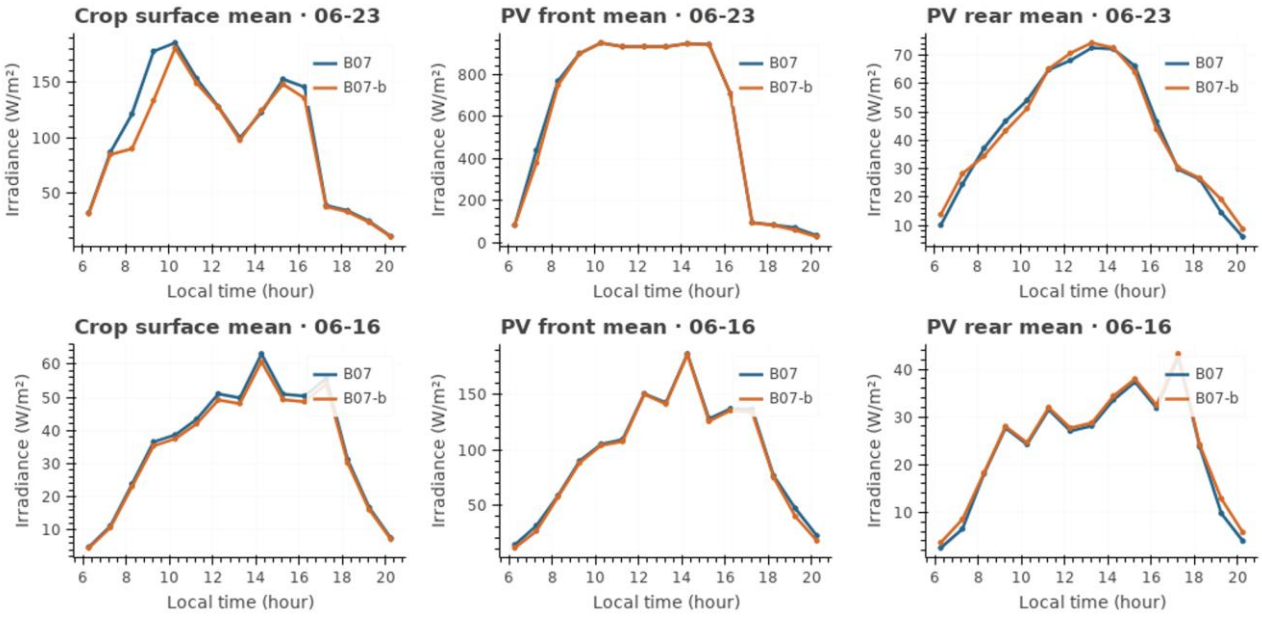


Figure 28: Module response on June example days. Upper row: clear-sky day 23 June. Lower row: overcast day 16 June.

On clear-sky day 23 June, the module change reduces crop irradiation by 7.03% and front irradiation by 1.20%, while rear irradiation increases by 1.07%. On overcast day 16 June, crop and front irradiation decrease by 3.39% and 2.47%, and rear irradiation increases by 3.96%. The crop reduction on both days indicates that the geometry affects diffuse access as well as direct shadows. The larger relative rear increase on the diffuse day is consistent with the annual sky-diffuse contribution, without implying that overcast conditions provide more absolute rear energy.

B13 — Crop count and rear irradiation

B13 increases Crop Model 1 from two to three objects per table at unchanged crop height. B07-b is the matching reference: both cases use Mono144 modules and share the same weather, timestamps, table positions, ground albedo and tracking settings. The population increases from 24 to 36 crops.

The agrivoltaic objective is to examine whether a denser under-row arrangement changes the mean light received by each unit of crop surface. The PV objective is to assess whether the additional crop geometry changes rear illumination by shading or obscuring reflecting surfaces. The comparison isolates crop count within the stated configuration; it does not compare different crop heights or PV module types.

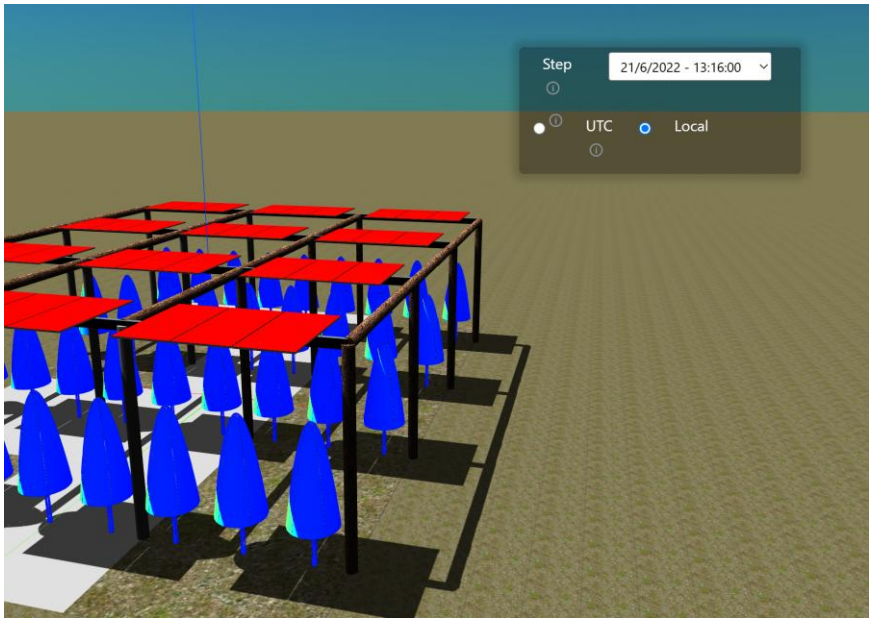


Figure 29: Three-crop configuration. B13 scene showing the denser planting arrangement. The image is labelled 21 June at 13:16 local time.

Receiving surface	B07-b two crops/table	B13 three crops/table	Change
Crop surface	326.80	318.75	−2.46%
PV front	1,443.73	1,443.80	+0.005%
PV rear	151.10	148.29	−1.85%

Table 12: Annual effect of increasing crop count

Annual crop irradiation decreases from 326.80 to 318.75 kWh/m² (−2.46%), while rear irradiation decreases from 151.10 to 148.29 kWh/m² (−1.85%). The PV-front change is +0.005%, which is negligible at the level of this assessment. The rear decrease of 2.80 kWh/m² occurs almost entirely in the reflected component; the sky contribution changes by only +0.003 kWh/m². This is consistent with additional crops changing the illuminated surfaces visible from the rear, rather than substantially changing its sky access.

The crop result is a mean per unit crop surface. Adding a third crop also increases the total represented crop area, so a 2.46% lower mean does not imply 2.46% less total intercepted energy across all crops. The representative-source mapping changes with crop count and contributes to the numerical comparison. Total interception, competition between plants and yield per unit land would require additional outputs and a crop model.

The matched pair therefore provides an optical indication of the consequences of denser planting beneath Mono144 tables. It does not identify the agronomically preferred planting density. The modest annual rear response should be evaluated alongside its seasonal distribution and the numerical sensitivity of rear irradiation.

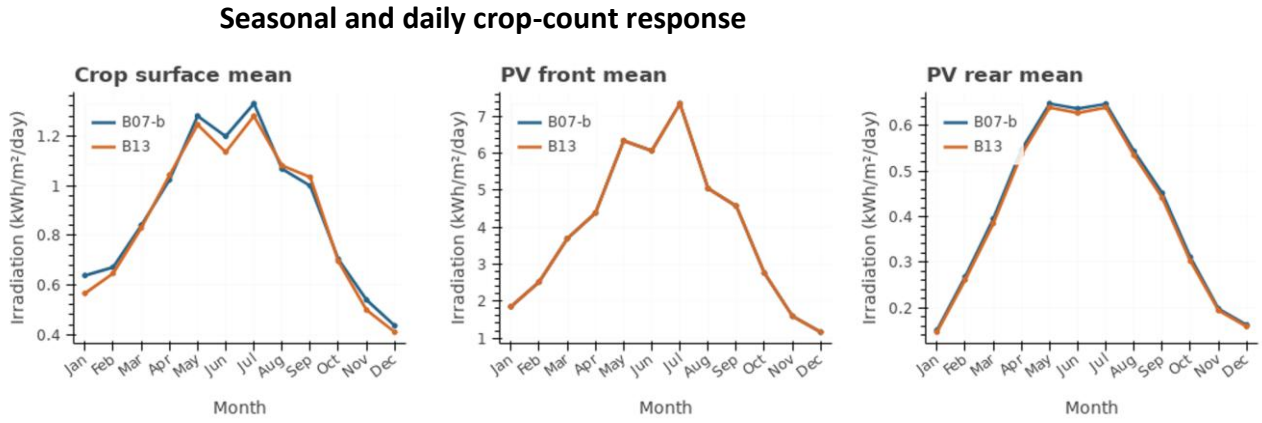


Figure 30: Monthly crop-count response. B13 versus B07-b, with Mono144 and Crop Model 1.

The crop mean decreases by 11.30% in January, 1.27% in March, 5.29% in June and 1.21% in October. Rear irradiation decreases by 2.72%, 2.58%, 1.50% and 2.75%, respectively, while front irradiation remains almost unchanged. The crop-light effect is therefore more seasonally variable than the rear response. For agrivoltaic planning, the relevance of the denser arrangement depends on the months in which light is required by the crop, rather than on the annual average alone.

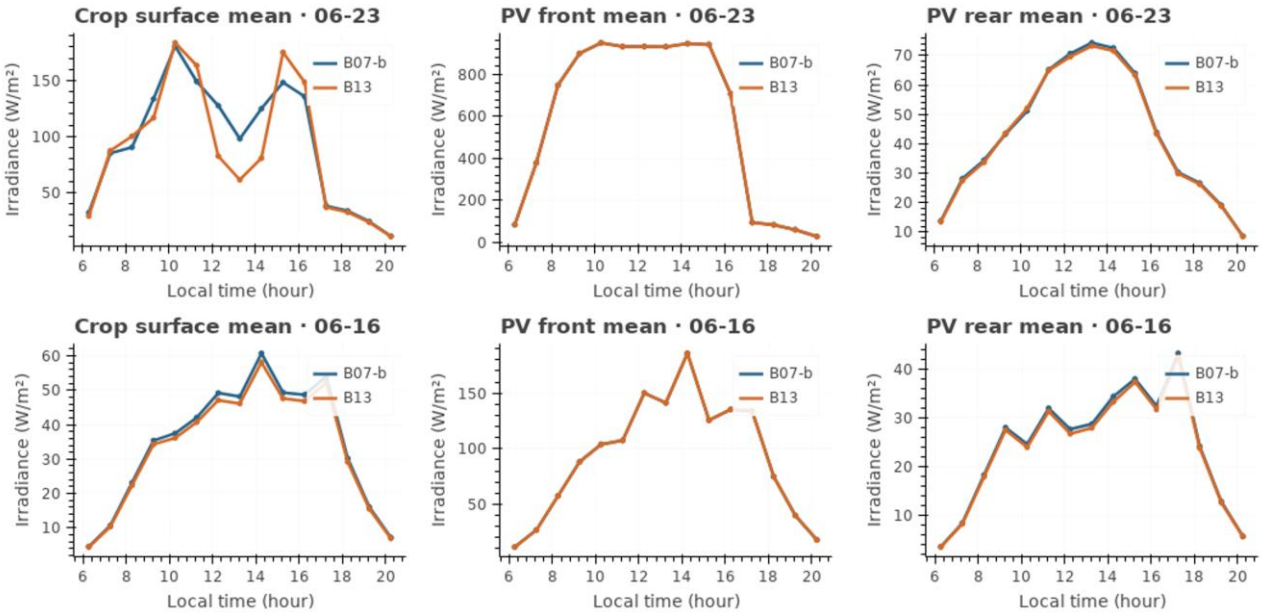


Figure 31: Crop-count response on June example days. Upper row: clear-sky day 23 June. Lower row: overcast day 16 June.

On clear-sky day 23 June, the third crop reduces mean crop irradiation by 5.70% and rear irradiation by 0.98%. On overcast day 16 June, the reductions are 3.64% and 2.17%. A crop response on the diffuse day indicates altered sky access and obstruction beyond direct shadows. The rear decrease on both days is consistent with changes to reflecting-surface visibility and illumination. These results connect planting density to the rear optical environment without establishing a corresponding electrical or crop-yield penalty.

B10–B12 — Complexity and computation time

The complexity cases assess how computational simplification changes the indicators used for early PV and agrivoltaic design. They change numerical settings, rather than the intended physical layout. B01 provides the high/high reference, with three PV representatives and five crop representatives. Both nominal surface resolution and representative-object reuse must be considered because they change together in this case set.

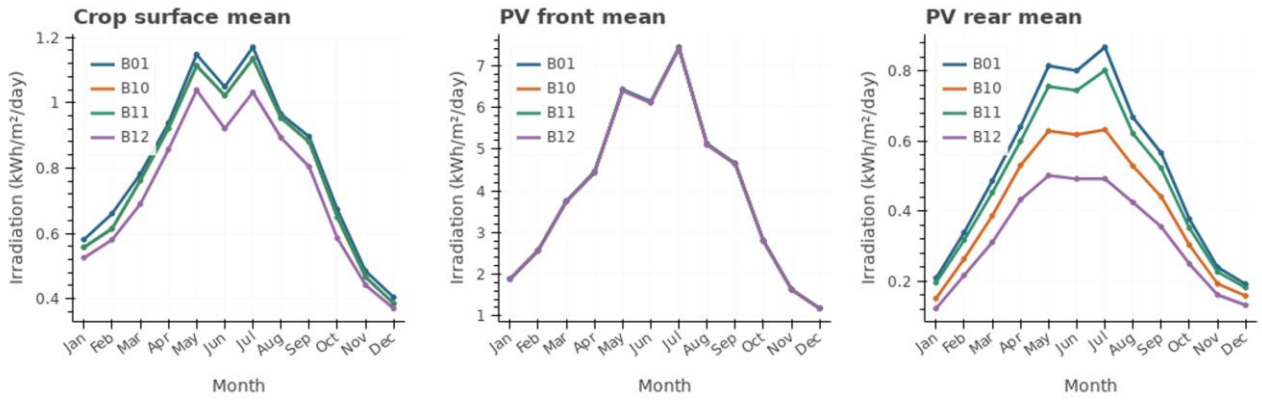


Figure 32: Monthly complexity comparison. B01 high/high compared with B10 low/high, B11 high/low and B12 low/low.

Case	Runtime min:s	Crop change	Front change	Rear change
B01	4:37	Reference	Reference	Reference
B10	3:03	-2.98%	-0.38%	-22.02%
B11	3:23	-2.98%	-0.33%	-6.90%
B12	1:31	-10.39%	-0.55%	-37.24%

Table 13: Complexity response relative to B01

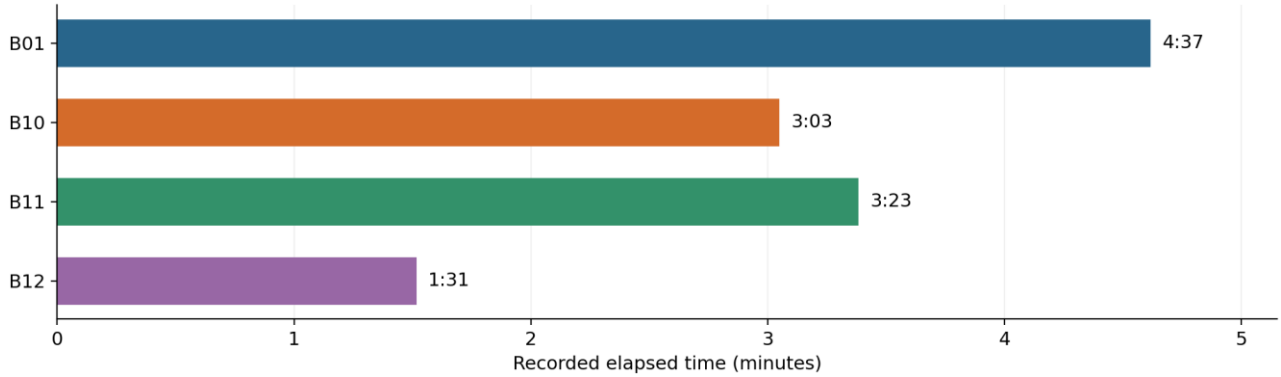


Figure 33: Recorded runtime for complexity settings. Each value is a single-run observation on the reference computer.

B10 uses low PV resolution (nominal 1 m spacing) and high crop resolution (0.25 m). Its runtime is 3 min 3 s, 33.9% below B01, while annual front, crop and rear irradiation differ by −0.38%, −2.98% and −22.02%. This is a substantial reduction in computation time, but the relatively small front difference would be a poor basis for assuming that the rear or crop outputs are equally stable.

B11 uses high PV resolution (0.25 m) and low crop resolution (1 m). It takes 3 min 23 s, 26.7% less time than B01, with front, crop and rear differences of −0.33%, −2.98% and −6.90%. Its rear result is closer to B01 than B10's. However, B10 and B11 both use one PV representative and five crop representatives, and their crop time series are identical. Effective crop receptor counts are not recorded, as highlighted in the methodology; this pair therefore does not establish a crop-mesh convergence trend.

B12 uses low PV and crop resolution, one PV representative and one crop representative, with values copied to the remaining targets. Its runtime falls to 1 min 31 s, a 67.1% reduction from B01. Front irradiation differs by −0.55%, but crop and rear irradiation differ by −10.39% and −37.24%. The smaller receptor workload explains its practical speed advantage, while the larger crop and rear differences limit the strength of design conclusions based on those outputs.

These values are differences from the high/high setting, not measured accuracy errors. Mesh resolution and representative-object selection are coupled, and B01 is not an independently converged solution. Rear modelling is particularly dependent on geometric and optical representation; comparisons of view-factor and ray-tracing models provide a broader methodological context for checking those assumptions [16], but do not validate the present configurable cases.

The appropriate setting therefore depends on the design question. A fast setting may support preliminary screening, but candidate designs should be reassessed at greater numerical detail when the decision depends on crop light or rear irradiation. The consistently small front differences do not demonstrate that simplified settings preserve an agrivoltaic trade-off involving other receiving surfaces.

Application runtime and hardware

Item	Specification
Operating system	Microsoft Windows 11
Processor	Intel Core i7-11370H at 3.30 GHz; 4 cores / 8 logical processors
RAM	16 GB
Installed graphics	NVIDIA GeForce MX450 and Intel Iris Xe Graphics

Table 14: Computer used for the simulations

Case	Elapsed time	Run type
B01	4 min 37 s	Single configuration
B02	4 min 57 s	Single configuration
B03	18 min 58 s	Pitch batch
B04	13 min 55 s	Tracker-height batch
B05	17 min 22 s	Crop-height batch
B06	5 min 2 s	Single configuration
B07	4 min 49 s	Single configuration
B07-b	5 min 20 s	Single configuration
B08	4 min 28 s	Single configuration
B09	4 min 36 s	Single configuration
B10	3 min 3 s	Single configuration
B11	3 min 23 s	Single configuration
B12	1 min 31 s	Single configuration
B13	5 min 54 s	Single configuration

Table 15: Recorded application runtime

Individual configurations take between 1 min 31 s and 5 min 54 s on the reference computer; B07-b takes 5 min 20 s. The batch observations are 18 min 58 s for B03, 13 min 55 s for B04 and 17 min 22 s for B05. They remain whole-batch times because shared calculations prevent assigning each total equally to its variants.

These observations indicate that the selected 12-table scenes can support iterative comparison within minutes on the study computer. In PV and agrivoltaic planning, this makes it practical to inspect several candidate geometries before selecting configurations for more detailed assessment. The value of a shorter run nevertheless depends on whether the crop and PV indicators remain sufficiently stable for the intended decision.

Discussion

Implications for early design

The configurable study shows that a parameter change can affect crops, PV fronts and PV rears differently. Backtracking gives a modest annual crop increase and a near-zero front change, while its rear response is larger. The seasonal and daily comparisons explain why an annual front value alone is insufficient: gains and losses can cancel, and the balance of direct, diffuse and reflected radiation changes with the weather sequence.

For PV design, these results identify changes in the incident resource that must subsequently be translated into electricity using appropriate module and system models. For agrivoltaics, they identify when and where crop surfaces receive light, which must be matched to canopy representation, cultivation periods and physiological demand. Maximising any one optical indicator does not by itself establish the best combined land use [14].

Greater pitch and tracker height increase mean crop and rear irradiation within their respective batches, whereas enlarging the uniformly scaled crop from 2 to 4 m reduces both. These responses describe the specified under-row planting arrangement. Wider pitch also changes the array footprint, greater tracker height has engineering implications, and larger crops have more total surface area. The comparisons therefore inform design choices without providing a universal ranking of layouts, planting densities or crop varieties.

Module selection and vegetation must be considered together in the rear assessment. With Crop Model 1, the larger Mono144 module reduces mean crop irradiation while increasing rear irradiation relative to Poly60. Adding a third crop per table produces a smaller rear decrease concentrated in the reflected component. The B06/B08 comparison separately identifies a ground-albedo effect under matched geometry. These results connect rear illumination to the full scene rather than to module bifaciality alone.

The comparisons are controlled within the references specified in Table 6. They are not a single ranking of all cases: crop populations, module types and tracking settings differ between some batches. Clear-sky day and overcast day examples refer to irradiance-based selections from a TMY, not confirmed historical observations of cloud cover. Their purpose is to explain the response under contrasting radiation conditions.

Use of irradiance outputs in crop models

LUSIM provides high-level broadband irradiance outputs that can be used as inputs to different crop models. Before this transfer, broadband irradiance must be converted into photosynthetically active radiation (PAR), following the methodology detailed in Deliverable D2.3 [6]. This links the configurable radiation assessment in Task 2.4 to the crop-response modelling developed elsewhere in SYMBIOSYST.

The receiving model may require PAR irradiance, photosynthetic photon flux density (PPFD) or daily light integral (DLI). The converted data must match its required units, time resolution and spatial definition. In particular, an area-weighted average over the external crop mesh is not automatically equivalent to irradiance on a horizontal canopy plane or to radiation absorbed by the canopy. The appropriate receptor or aggregation must be selected before transferring the data.

The present outputs therefore describe an input to agronomic assessment, not a crop-yield prediction. Crop development, radiation-use processes, temperature, water and other environmental or management inputs remain the responsibility of the receiving crop model. This distinction is necessary when interpreting a percentage change in broadband crop irradiation as a potential agricultural benefit or constraint.

Limitations

The assessment uses generic static crop shapes, a flat horizon, a finite 12-table array and one TMY sequence. It does not represent seasonal canopy development, crop physiological adaptation, climate extremes or interannual variability. A valid no-PV reference is not available in this version of the demo tool, therefore crop irradiation is compared with PV-equipped reference scenes rather than open-field light availability. Neither crop yield nor land-normalised electrical energy is calculated.

The highlighted checks identify the remaining data limitations: incomplete B06 front and crop components; verification that B08 front and crop exports match its rear run; the reflecting surfaces included in the exported Albedo term; effective crop receptor meshes for B10 and B11; and reconciliation of the archived weather file with the weather columns used in the simulations. Conclusions are restricted to the supported outputs. The user-confirmed geometry and material settings are retained as specified.

Numerical limitations include surface sampling, representative-object copying and interpolation from 12 representative days and five tracker angles. The complexity cases show greater sensitivity in rear and crop irradiation than in PV-front irradiation, but do not separate the effects of mesh resolution and representative selection. Agreement between time-series integration and summary exports establishes internal consistency, not physical validation. D2.2 provides validation and benchmarking of the underlying approaches [10]; no independent measured or solver reference is included for these configurable cases. Mechanistic explanations remain conditional where angle histories or individual reflecting-surface contributions are unavailable.

Aerial Agri-Topography: UAV-derived site models for Agri-PV early design

Introduction

Above Surveying (ABOVE) contributes to Task 2.4 with a UAV-based survey and processing workflow that converts orthomosaic imagery and photogrammetric 3D models of an Agri-PV site into geometric information for early design. Under the Grant Agreement, ABOVE develops a tool based on orthomosaic images and 3D models of the aerial agrivoltaic topography of prospective sites, supporting the creation of 3D models for Agri-PV designs where modules are mounted higher above the ground than in conventional PV plants. The full acquisition specification and methodology are reported in Deliverable D3.2; this section summarises the topographic and 3D modelling work and the results obtained at the Bolzano demonstrator.

The contribution addresses three questions:

• Which survey specification yields terrain, crop and structure geometry at a resolution suitable for Agri-PV design?

• Which data products result, and with what accuracy?

• How can these products inform early design decisions, and with what limits?

Methodology

The survey uses RGB imagery from a survey-grade mapping camera on any suitable drone, with RTK corrections recommended. Surveyed ground control points (GCPs) are mandatory regardless of image geotagging, because absolute vertical accuracy cannot be established from platform-recorded positions alone. Large sites may be covered in several flights, limited only by platform endurance. Table 16 gives the general requirement alongside the setting used at Bolzano. Where airspace restrictions prevent the altitude needed to meet the specified GSD and overlap, a site-specific deviation is recorded.

Parameter	Requirement	Bolzano campaign
Platform and payload	Drone with survey-grade RGB mapping camera and mechanical shutter	Soleon Coanda x6; Ricoh GR on Riegl miniVUX-1UAV payload (LiDAR not processed)
GSD and altitude	Finer than 3 cm/pixel, within airspace limits	0.5 cm/pixel reported at approx. 45 m AGL.
Overlap and oblique	80 % front and side; smart oblique on where a 3D model is required	As specified; 3D model produced
Camera settings	4:3 JPEG; ISO 100 (200 max); shutter faster than 1/320 s; EV adjusted based on available lighting.	As specified
Georeferencing	RTK or NRTK GNSS; ≥ 4 checkerboard GCPs of ≥ 50 × 50 cm; < 3 cm 3D RMSE	Leica GS18 in NRTK; 6 GCPs; ≤ 1 cm 3D RMSE

Table 16: Topographic survey specification and Bolzano campaign settings

Images are aligned and orthorectified with a structure-from-motion pipeline (Agisoft Metashape) to produce a georeferenced RGB orthomosaic. A digital surface model (DSM) is generated from the tie point cloud, and ground points are classified to produce a digital terrain model (DTM). Three further products are specific to Agri-PV: **CAD line work** placing crop positions (at Bolzano, individual apple trees) and PV support structures in one georeferenced drawing; a **correlation of surveyed structure positions** with structural CAD where available; and, with oblique acquisition, a **textured 3D site model** containing both PV modules and trees. Outputs are hosted in the ABOVE SolarGain portal as map layers and downloadable artefacts: the orthomosaic as GeoTIFF, terrain models as TIN surfaces, CAD line work as DWG/DXF and the 3D model as OBJ, STL or Cesium 3D Tiles.

Results

The Bolzano demonstrator comprises 200 Aleo modules (74.6 kWp) on single-portrait trackers in seven rows over apple trees: 140 opaque 415 W modules and 60 semi-transparent 275 W modules with approximately 60 % transparency. The topographic dataset was acquired on 2 June 2026. The RGB images produced the orthomosaic, DSM, CAD line work and a 3D site model. The line work marks each

apple tree and support structure together with contour lines (Figure 34), and the 3D model represents both the PV modules and the tree structures (Figure 35). The GNSS survey of the GCPs achieved ≤ 1 cm 3D RMSE.

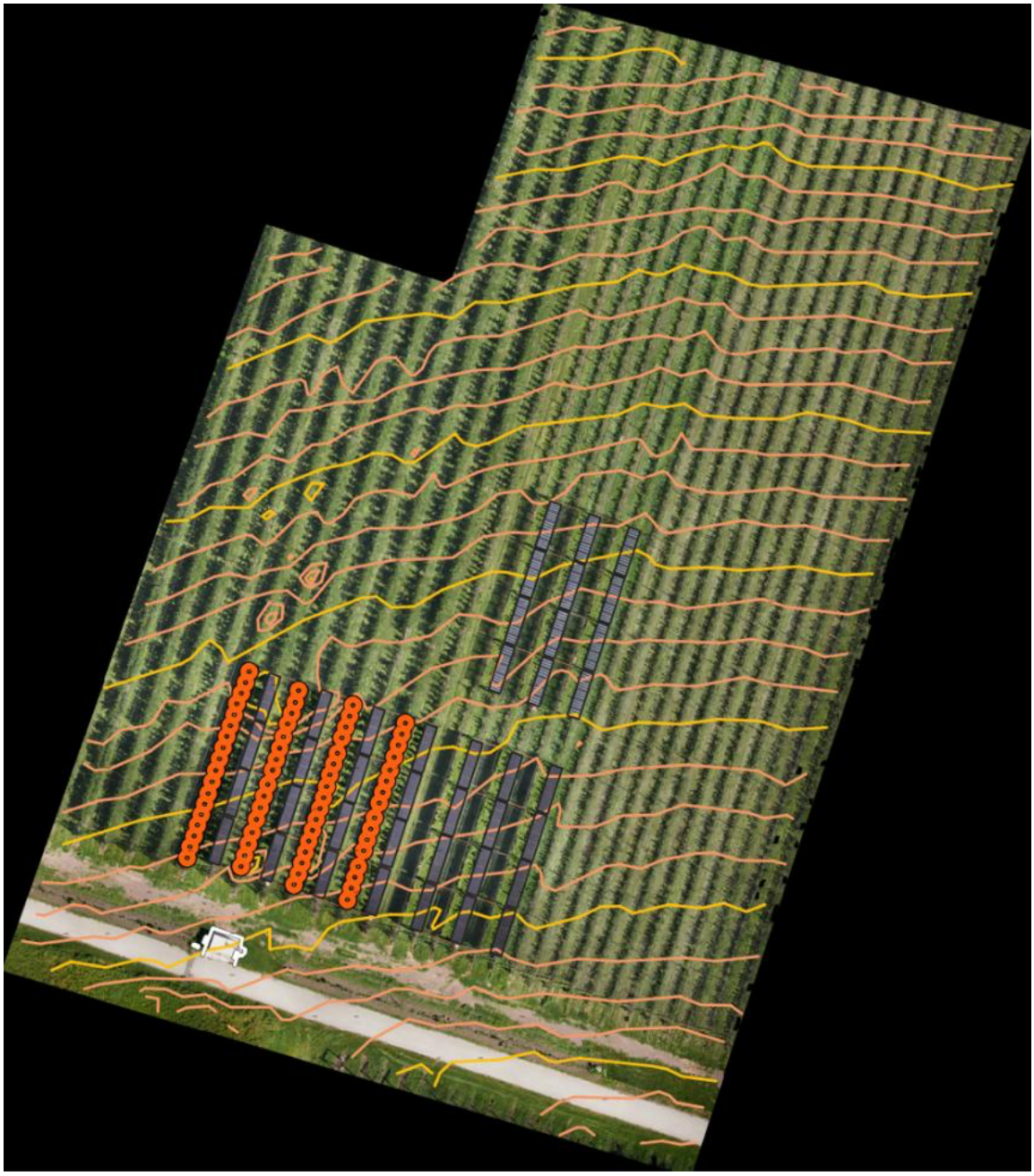


Figure 34: Topographic map of the Bolzano demonstrator with apple tree positions and contour lines [17].

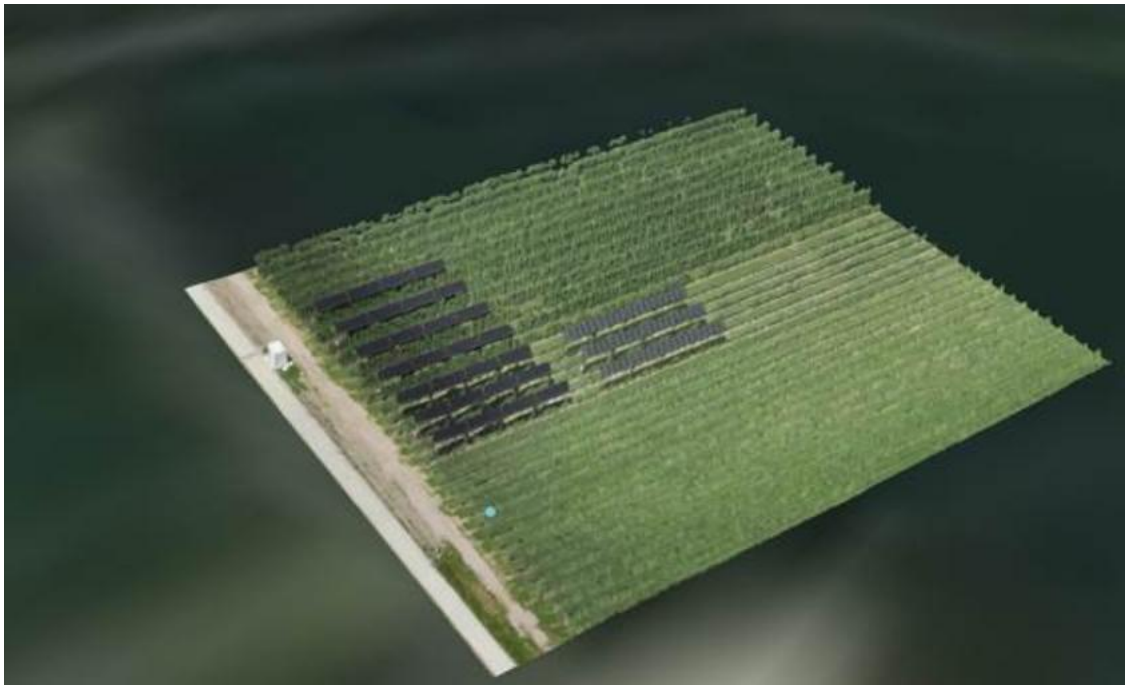


Figure 35: 3D model of the Bolzano demonstrator showing PV modules and tree structures [17].

Discussion

The products give measured rather than estimated site geometry at the start of design. Tree positions in the CAD line work show what the support structures must work around and give the proportion of bare soil to plant cover beneath the modules, which is relevant to table layout and to estimating rear-side gain. The terrain model shows the ground on which foundations sit and supports the choice of structure heights and positions over an established crop. The textured 3D model provides a georeferenced as-built scene that can serve as the basis for design studies and preliminary lighting assessment in general CAD software.

Limitations. Ground classification beneath dense canopy and module tables can introduce errors of a few centimetres into the DTM; stowing trackers during the survey partly mitigates this, and at Bolzano the LiDAR data that could improve sub-canopy terrain were not processed. Where pseudo-GCPs replace permanent targets, later campaigns inherit the accuracy of the first. The models are snapshots of the survey date and do not capture seasonal canopy change. No preliminary lighting simulation on the Bolzano model is reported in D3.2.

Conclusions

This deliverable has presented the **DualHarvest** (Agri-PV Early Design Tool) together with the **LUSIM demonstrator environment** as complementary modelling solutions developed within the SYMBIOSYST project to support early-stage assessment of agrivoltaic systems. DualHarvest enables rapid and flexible screening of Agri-PV configurations by providing simplified estimates of both photovoltaic energy production and irradiance distribution on crops, while LUSIM allows a more detailed spatial and temporal visualisation of irradiance patterns in representative demonstrator cases. Together, these tools establish a coherent workflow that supports the preliminary exploration of design options and the understanding of key trade-offs between agricultural and energy performance.

The modelling framework described in this report highlights the importance of integrating **radiation modelling with agronomic interpretation**, enabling users to move from physical irradiance outputs to crop-relevant indicators such as PAR, PPFD, and DLI. This connection is essential to ensure that early-stage design choices remain consistent with crop-specific light requirements and agricultural objectives. In this context, the tools contribute to improving the transparency and accessibility of agrivoltaic design processes for a broad range of stakeholders, including farmers, agronomists, project developers, and policymakers.

At the same time, it is important to emphasise that DualHarvest and LUSIM are early-stage support tools, based on simplified modelling approaches and predefined assumptions. Their outputs should not be interpreted as final design solutions, but rather as indicative results to guide further analysis. Co-design must therefore be regarded as a foundational principle of any agrivoltaic project. Engineering choices should be developed in continuous alignment with agronomic needs and constraints, and vice versa, particularly with reference to the operational phase of the installation. Integrated design workflows—supported by appropriate modelling tools—ensure that energy generation, agricultural performance, and long-term land stewardship remain balanced and mutually reinforcing throughout the project lifecycle. The responsible use of these tools requires users to combine model outputs with site-specific data, agronomic expertise, and detailed technical assessments, including aspects such as crop management, local climate conditions, engineering design, grid connection, and regulatory frameworks.

In conclusion, the DualHarvest tool and the LUSIM demonstrator represent a significant step towards the development of accessible and scientifically grounded tools for agrivoltaic system design. By supporting informed decision-making at the early stages of project development, they contribute to reducing uncertainty and risks, improving design coherence, and fostering the adoption of agrivoltaics as a viable and sustainable land-use solution. Future developments may further enhance these tools through the integration of more advanced agronomic models, expanded scenario capabilities, and closer coupling with real-world monitoring data from SYMBIOSYST demonstrators.

ABOVE has specified and demonstrated a UAV topographic survey workflow that captures Agri-PV sites at centimetre resolution with surveyed ground control. At the Bolzano demonstrator it produced an orthomosaic, terrain models, CAD line work locating every apple tree and support structure, and a textured 3D site model. These outputs provide measured site geometry for early Agri-PV design, particularly where installations are planned over existing crops.

References

[1] D.L. King, W.E. Boyson, J.A. Kratochvill, 'Photovoltaic Array Performance Model', SANDIA, Dec. 2004.

[2] R. W. Thimijan and R. D. Heins, 'Photometric, Radiometric, and Quantum Light Units of Measure: A Review of Procedures for Interconversion', *HortScience*, vol. 18, no. 6, pp. 818–822, Dec. 1983, doi: 10.21273/HORTSCI.18.6.818.

[3] Reher Thomas, 'Agrivoltaics: optimizing the synergy of crop production and solar panels'.

[4] O. D. Palmitessa, P. Paciello, and P. Santamaria, 'Supplemental LED Increases Tomato Yield in Mediterranean Semi-Closed Greenhouse', *Agronomy*, vol. 10, no. 9, p. 1353, Sep. 2020, doi: 10.3390/agronomy10091353.

[5] S. Cruz and C. Gómez, 'Effects of Daily Light Integral on Compact Tomato Plants Grown for Indoor Gardening', *Agronomy*, vol. 12, no. 7, p. 1704, Jul. 2022, doi: 10.3390/agronomy12071704.

[6] SYMBIOSYST Deliverable D2.3. Broadband-to-PAR conversion methodology.

[7] SYMBIOSYST Deliverable D6.2. Simplified Model to Reach Broader Stakeholders Audience.

[8] J. Robledo, J. Leloux, E. Lorenzo and C. A. Gueymard, "From video games to solar energy: 3D shading simulation for PV using GPU", Solar Energy, vol. 193, pp. 962–980, 2019. https://doi.org/10.1016/j.solener.2019.09.041.

[9] J. Robledo, J. Leloux, B. Sarr, C. A. Gueymard, A. Driesse and P.-F. Drouin, "Simulating the energy yield of bifacial photovoltaic modules installed on carports or canopies", 38th European Photovoltaic Solar Energy Conference and Exhibition, pp. 1583–1587, 2021.

[10] SYMBIOSYST, Deliverable D2.2: Validation and benchmark of modelling tools for light assessment using ray-tracing and GPU-based method, 30 December 2024, Sections 2.1–2.3 and 7.

[11] J. E. Hay and J. A. Davies, "Calculations of the solar radiation incident on an inclined surface", in Proceedings of the First Canadian Solar Radiation Data Workshop, J. E. Hay and T. K. Won, Eds., Ministry of Supply and Services, Canada, 1980. Method reference: https://pvlib-python.readthedocs.io/en/stable/reference/generated/pvlib.irradiance.haydavies.html.

[12] E. Lorenzo, L. Narvarte and J. Muñoz, "Tracking and back-tracking", Progress in Photovoltaics: Research and Applications, vol. 19, pp. 747–753, 2011. https://doi.org/10.1002/pip.1085.

[13] M. A. Anoma et al., "View Factor Model and Validation for Bifacial PV and Diffuse Shade on Single-Axis Trackers", in 2017 IEEE 44th Photovoltaic Specialist Conference (PVSC), pp. 1549–1554, 2017. https://doi.org/10.1109/PVSC.2017.8366704.

[14] C. Dupraz et al., "Combining solar photovoltaic panels and food crops for optimising land use: Towards new agrivoltaic schemes", Renewable Energy, vol. 36, pp. 2725–2732, 2011. https://doi.org/10.1016/j.renene.2011.03.005.

[15] H. Marrou, J. Wery, L. Dufour and C. Dupraz, “Productivity and radiation use efficiency of lettuces grown in the partial shade of photovoltaic panels”, European Journal of Agronomy, vol. 44, pp. 54–66, 2013. https://doi.org/10.1016/j.eja.2012.08.003.

[16] M. Ernst, C.-A. Asselineau, P. Tillmann, K. Jäger and C. Becker, “Modelling bifacial irradiance – Step-by-step comparison and validation of view factor and ray tracing models”, Applied Energy, vol. 369, article 123574, 2024. https://doi.org/10.1016/j.apenergy.2024.123574.

[17] SYMBIOSYST, Deliverable D3.2: Description of innovative sensors, metrology, and O&M platforms for agri-PV solutions, 2026, chapters “UAV-Based Aerial Monitoring and Imaging (ABOVE)” and “UAV-Based Digital Solutions (ABOVE)”.